

AD-A038 980

SOUTHWEST RESEARCH INST SAN ANTONIO TEX
DEVELOPMENT OF DIAGNOSTIC TEST EQUIPMENT FOR INSPECTING ANTIFRI--ETC(U)
MAR 77 F N KUSENBERGER, J R BARTON
SWRI-15-3764 AMMRC-CTR-77-13 DAA646-74-C-0012

F/G 13/9

UNCLASSIFIED

NL

1 of 1
AD
A038980



END

DATE
FILMED
5-77

ADA 038980



12

AD

[Handwritten signature]

AMMRC CTR 77-13

DEVELOPMENT OF DIAGNOSTIC TEST EQUIPMENT FOR INSPECTING ANTI-FRICTION BEARINGS

March 1977

Felix N. Kusenberger
John R. Barton
Southwest Research Institute
P.O. Drawer 28510
San Antonio, Texas 78284



Final Report Contract Numbers DAAG46-74-C-0012
DAAG46-75-C-0001

Approved for public release; distribution unlimited

Prepared for
U.S. ARMY AVIATION SYSTEMS COMMAND
St. Louis, Missouri 63166

ARMY MATERIALS AND MECHANICS RESEARCH CENTER
Watertown, Massachusetts 02172

DDC FILE COPY,



SOUTHWEST RESEARCH INSTITUTE
SAN ANTONIO CORPUS CHRISTI HOUSTON

The findings in this report are not to be construed as an official Department of the Army position, unless so designated by other authorized documents.

Mention of any trade names or manufacturers in this report shall not be construed as advertising nor as an official indorsement or approval of such products or companies by the United States Government.

DISPOSITION INSTRUCTIONS

**Destroy this report when it is no longer needed.
Do not return it to the originator.**

UNCLASSIFIED

SECURITY CLASSIFICATION OF THIS PAGE (When Data Entered)

REPORT DOCUMENTATION PAGE		READ INSTRUCTIONS BEFORE COMPLETING FORM																
1. REPORT NUMBER 18 AMMRC CTR-77-13 ✓	2. GOVT ACCESSION NO.	3. RECIPIENT'S CATALOG NUMBER																
4. TITLE (and Subtitle) DEVELOPMENT OF DIAGNOSTIC TEST EQUIPMENT FOR INSPECTING ANTI-FRICTION BEARINGS ✓		5. TYPE OF REPORT & PERIOD COVERED Final Report, Sept. 19, 1973 to Feb. 28, 1977 ✓																
7. AUTHOR(s) 19 Felix N. Kusenberger John R. Barton		6. PERFORMING ORG. REPORT NUMBER 15-3764 and 15-4052 ✓																
9. PERFORMING ORGANIZATION NAME AND ADDRESS Southwest Research Institute ✓ 8500 Culebra Rd., P.O. Drawer 28510 San Antonio, Texas 78284		8. CONTRACT OR GRANT NUMBER(s) DAAG46-74-C-0012 <i>new</i> DAAG46-75-C-0001																
11. CONTROLLING OFFICE NAME AND ADDRESS U.S. Army Aviation Systems Command P.O. Box 209 St. Louis, Mo 63166		10. PROGRAM ELEMENT, PROJECT, TASK AREA & WORK UNIT NUMBERS AMCMS Code: 738017, A50Q 3019 IGL 3GL																
14. MONITORING AGENCY NAME & ADDRESS (if different from Controlling Office) Army Materials and Mechanics Research Center Watertown, Massachusetts 02172		12. REPORT DATE 11 March 1977 ✓																
		13. NUMBER OF PAGES 81 <i>(2) 78p-1</i>																
		15. SECURITY CLASS. (of this report) Unclassified																
		15a. DECLASSIFICATION/DOWNGRADING SCHEDULE																
16. DISTRIBUTION STATEMENT (of this Report) 14 SWRI-15-3764, SWRI-15-4052 Approved for public release; distribution unlimited.																		
17. DISTRIBUTION STATEMENT (of the abstract entered in Block 20, if different from Report) 9 Final rept. 19 Sep 73- 28 Feb 77, 328 200																		
18. SUPPLEMENTARY NOTES																		
19. KEY WORDS (Continue on reverse side if necessary and identify by block number) <table style="width: 100%; border: none;"> <tr> <td style="width: 33%;">Nondestructive Testing</td> <td style="width: 33%;">Life expectancy</td> <td style="width: 33%;">Bearings</td> </tr> <tr> <td>Magnetic detectors</td> <td>Reliability</td> <td>Antifriction bearings</td> </tr> <tr> <td>Magnetic signatures</td> <td>Detection</td> <td>Stresses</td> </tr> <tr> <td>Barkhausen Effect</td> <td>Inspection</td> <td>Residual stress</td> </tr> <tr> <td></td> <td></td> <td>Defects (materials)</td> </tr> </table>				Nondestructive Testing	Life expectancy	Bearings	Magnetic detectors	Reliability	Antifriction bearings	Magnetic signatures	Detection	Stresses	Barkhausen Effect	Inspection	Residual stress			Defects (materials)
Nondestructive Testing	Life expectancy	Bearings																
Magnetic detectors	Reliability	Antifriction bearings																
Magnetic signatures	Detection	Stresses																
Barkhausen Effect	Inspection	Residual stress																
		Defects (materials)																
20. ABSTRACT (Continue on reverse side if necessary and identify by block number) (see reverse side)																		

lps

20. Abstract

Historical background summarizing the need for improved non-destructive inspection of antifriction bearings is presented. A state-of-the-art computer supervised semi-automated bearing inspection system is described which incorporates the magnetic perturbation method for surface and subsurface flaw detection and the Barkhausen noise method for assessing the state of stress in the active regions of the raceway. The capabilities and features of the inspection system are presented along with verification test data comparing results from a preliminary prototype unit and a prototype system. Other inspection data from used and refurbished bearing races are summarized. Metallurgical sectioning and endurance test results are included which verify the flaw detection capability of the system and establish the capability of the system to detect subsurface flaws which cause failure. Highlights of system development are also briefly summarized.

PREFACE

Funding and guidance for this work was provided by the Army Aviation Systems Command (AVSCOM), St. Louis, Missouri. The AMMRC Contract Manager was Mr. Harold Hatch, DRXMR-MI. Mr. Hugh Bull, DRSAV-FESI, of AVSCOM at the Corpus Christi Army Depot (CCAD) provided guidance during the installation and acceptance phases at that installation. Appreciation is expressed to both Mr. Hatch and Mr. Bull for their excellent guidance and cooperation throughout the program for the development of the bearing inspection system.

ACCESSION for		Write Section <input checked="" type="checkbox"/>
		Buff Section <input type="checkbox"/>
RTIS		
DOC		
UNANNOUNCED JUSTIFICATION		
BY DISTRIBUTION/AVAILABILITY CODES		
Dist.	AVAIL. and/or	SPECIAL
A		

TABLE OF CONTENTS

	<u>Page</u>
I. INTRODUCTION	1
II. PROTOTYPE INSPECTION SYSTEM	9
A. Description	9
B. Capabilities	16
III. INSPECTION DATA AND RESULTS	21
A. Verification Cross-Check	21
B. Refurbished Bearing Inspection (Using Laboratory Apparatus)	23
C. Additional Bearing Inspection (Preliminary Prototype Unit)	34
D. Metallurgical Sectioning	36
IV. OTHER RELATED RESULTS	45
V. CONCLUSIONS AND RECOMMENDATIONS	49
VI. REFERENCES	51
APPENDIX - Bearing Inspection Equipment Development Highlights	52

I. INTRODUCTION

Since the late 1950's, there has been an increasing need for improved, more definitive nondestructive inspections for bearings used in critical applications. This need has been accentuated by the evolution of the gas turbine engine, high performance aircraft, helicopters, rocket engines, satellites, etc. Furthermore, advanced technology engines, currently under development, increase the demands on bearings which intensifies the need for critical inspection equipment. Common, presently used inspection practices consist of a meticulous visual examination, at approximately 10X magnification, and the use of a radius scribe to assess the severity of surface imperfections, stylus measurement of surface finish, and mechanical measurements of size and geometry. Even with such extensive inspections, improvements are critically needed. In particular, present inspection practices used both during manufacture and overhaul are completely incapable of finding minute, surface and subsurface inclusions of the order of 0.001-inch (0.025 mm) in diameter and there is no routine determination of residual stress conditions in either new or used bearings nor any monitoring of stress changes that may occur as a result of service. Research studies have shown that both minute inclusions as well as residual stress conditions are extremely important to the life of antifriction bearings.

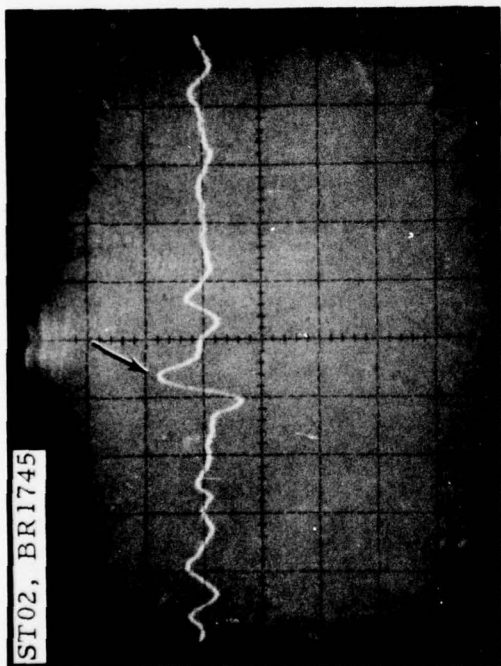
Since 1957, under the sponsorship of General Motors, the Navy, and the Air Force, Southwest Research Institute has developed non-destructive inspection methods for bearings which now provide a significantly improved inspection procedure. Over the past several years, discussions with personnel of the Army, Navy, Air Force, and commercial airlines have resulted in the evolution of concepts for incorporating the improved methodology into an integrated program with the acronym CIBLE - Critical Inspection of Bearings for Life Extension.

The detection of minute, surface and subsurface inclusions in the active regions of bearing races is now possible on a routine basis using the magnetic perturbation method. Magnetic perturbation inspection consists of applying radially and circumferentially oriented magnetic fields to a bearing component and sensing disturbances in these applied fields caused by flaws such as inclusions, pits, indents, cracks, etc. in the component. Radial field inspection is primarily sensitive to surface imperfections while circumferential field yields more sensitivity to defects near but beneath the surface. The strength of the applied field is also important. Inspections conducted with strong applied fields (near magnetic saturation) provide excellent

sensitivity to geometrical type flaws (inclusions, pits, etc.); similar inspections conducted at reduced fields enhance the detectability of flaws having associated localized stresses (fatigue cracks, indents, etc.). Figure 1 illustrates the direct correlation which has been obtained between circumferential signals and corresponding inclusions through metallurgical sectioning. The inspection signature obtained from the flaw is pointed out by the arrow in the signal trace at the top of Figure 1. The photomicrographs at the bottom of the figure show the flaw which generated the signature, obtained by meticulous metallurgical sectioning of the bearing race at the location from which the signature was obtained. The average diameter of the flaw illustrated in Figure 1 is slightly less than 0.001-inch (0.025 mm).

Residual stress conditions in the active region of the raceway can also be readily sampled utilizing the Barkhausen phenomena. From modern magnetic domain theory, the small, abrupt, discontinuous increments noted in the magnetization of a ferromagnetic material by Barkhausen in 1917, known as Barkhausen jumps, are now recognized as discontinuous movements of the mobile boundaries (Block walls) between adjacent domains. It has been established that both the direction and magnitude of mechanical stress in a ferromagnetic specimen strongly influences the dynamics of domain wall motion, thus influencing the Barkhausen effect.

In practice, a time-varying controlled magnetization is applied to the bearing race, and the changes which occur in the magnetic domain configuration are sensed with a probe. Several typical Barkhausen signatures obtained by electronically processing the "Barkhausen noise" picked up by the probe are illustrated in Figure 2. The signatures were obtained from the loaded and nonloaded halves of the inner race of a J85 engine main shaft bearing before service (new) and after approximately 1,000 hours of service. The two records at the right of Figure 2 obtained from the nonloaded side of the race show essentially no change as a result of service as anticipated since the balls do not run over this region of the raceway; the elapsed time between "before" and "after" service records was almost 2-1/2 years. The two records in the left of the figure illustrate what can take place as a result of service on a bearing; notice the region pointed out by the arrows in each of the records which show the development of a "spike" near the leading edge of the Barkhausen signature. Such "spike" signals have been observed on bearings after as few as 20 hours of service and on other bearings with in excess of 1,000 hours of service no spikes have developed. The formation of a "spike" is attributed to the development of a subsurface residual tensile stress region which reduces the compressive stresses initially introduced in



Location A Signature

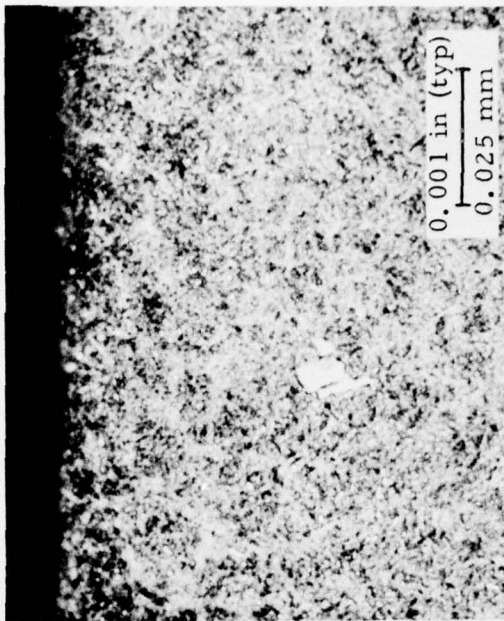
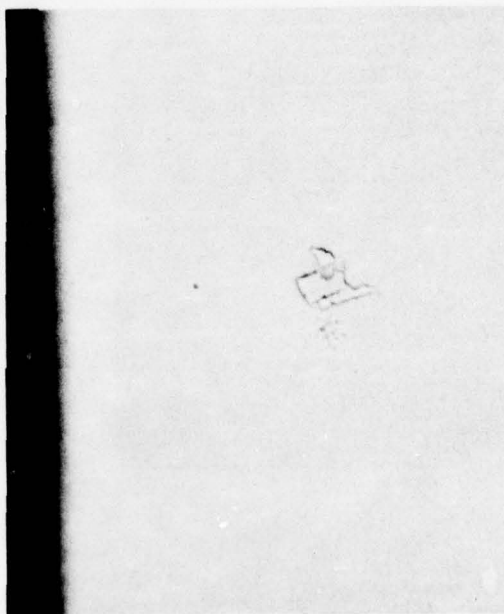
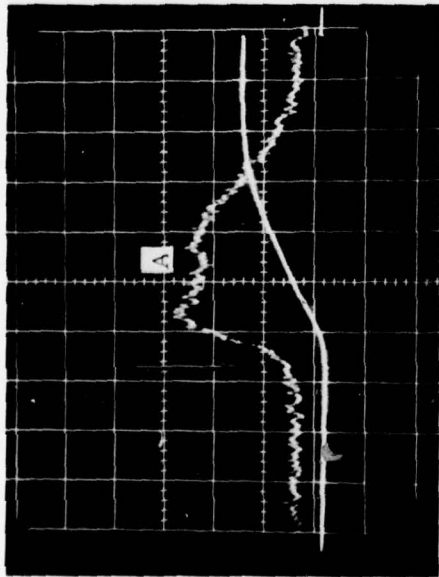


FIGURE 1. MAGNETIC PERTURBATION CIRCUMFERENTIAL SIGNATURE AND CORRESPONDING SUBSURFACE FLAW, P/N 1-300-015, S/N 470V(2) INNER RACE (HALF)

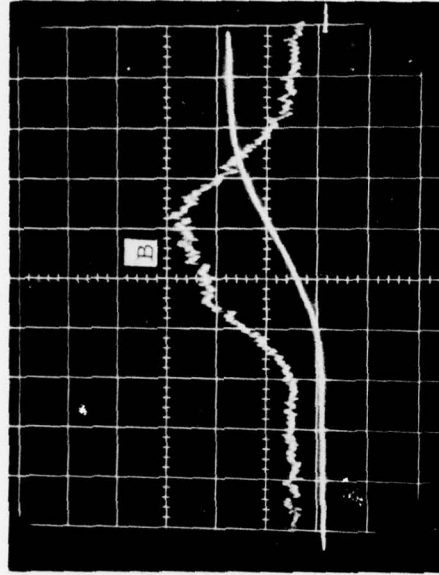
2698

Loaded Side of Raceway
Location 2 (Arbor 0°, Probe 28.5°)

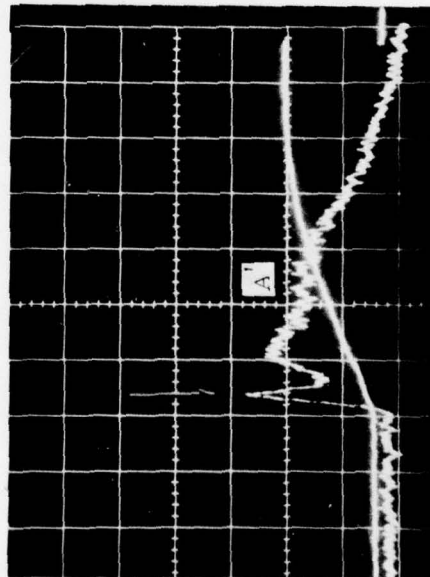


0 hours

Nonloaded Side of Raceway
Location 3 (Arbor 0°, Probe 331.5°)



Location 2



986 hours

Location 3

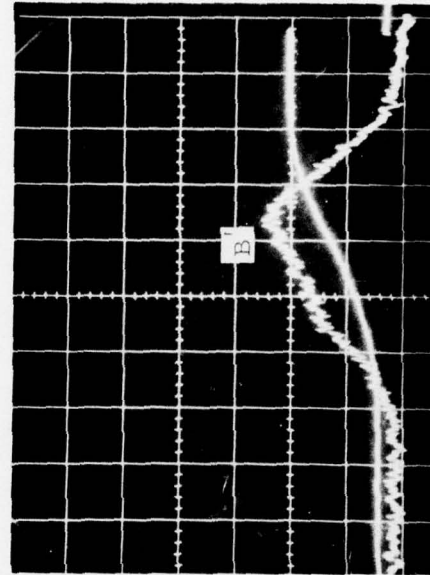


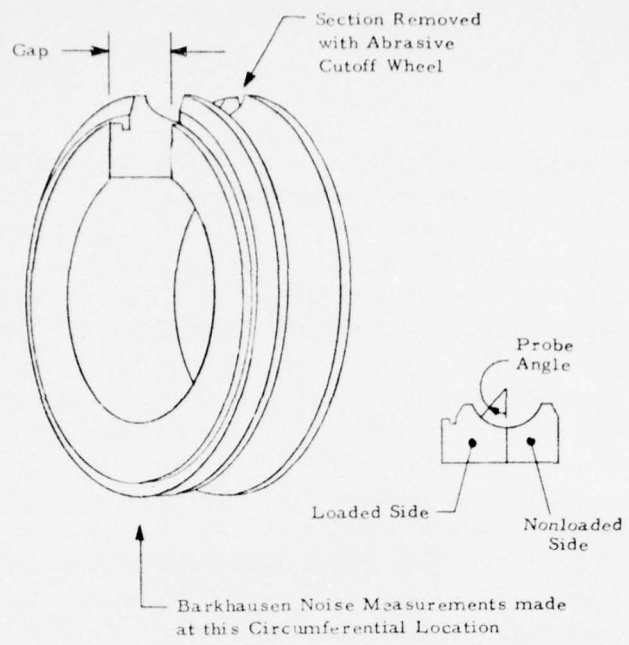
FIGURE 2. TYPICAL BARKHAUSEN RECORDS BEFORE AND AFTER APPROXIMATELY 1000 HOURS SERVICE ON A J85 MAIN SHAFT BEARING (S/N 07257)

the bearing to improve its fatigue life. This conclusion is supported by recently reported data. (1)* Furthermore, qualitative results obtained during applied stress experiments conducted on a bearing race show signature changes similar to the service bearing. These results are presented in Figures 3A and 3B. The data in Figure 3 were obtained from the ball groove surface (outer surface) on the inner race of a failed J85 main shaft bearing; extensive surface damage was present in the ball groove region of both nonloaded and loaded halves of this inner race. Notice a leading edge "spike" is present on three locations across the race in the "as received" condition prior to cutting the specimen. Subsequently, a section was cut from the race to facilitate modifying the net section stress via bending. The lower row of records in Figure 3A, obtained after cutting (without applying any bending moment) shows a decrease in the amplitude of the "spike" signal for nearly all nonloaded side locations. When tension is applied (i. e., reduction of the gap) the "spike" signal amplitude becomes greater than that obtained after cutting the race (compare top row of records in Figure 3B with the bottom row of records in Figure 3A). Importantly, the application of tensile stresses produces signature shapes similar to that for some bearings after service (reference lower left record in Figure 2). Alternatively, the application of compressive stress causes the leading edge spike signal to decrease for all locations, see lower two rows of records in Figure 3B. Other magnetic perturbation and Barkhausen signatures along with a detailed account of the manner in which these were obtained are presented in this report.

The development of a bearing inspection equipment incorporating magnetic perturbation for detecting surface and subsurface flaws in antifriction bearing races was initiated in September of 1973 under Contract DAAG46-74-C-0012. In August 1974, addition of residual stress measuring capabilities to the magnetic perturbation inspection equipment was initiated under Contract DAAG46-75-C-0001. Although development of the magnetic perturbation and Barkhausen noise inspection equipment has proceeded under two contracts, the result is a unified bearing inspection system incorporating the two methods.

A preliminary prototype unit was constructed and operated to prove out the crucial elements of the overall system engineering design. A prototype inspection system was subsequently developed based on the experience gained from the preliminary unit. The prototype inspection system was installed in the Bearing Inspection Facility at the Corpus

* Superscript numbers in parentheses refer to list of references at the end of this report.



3336a

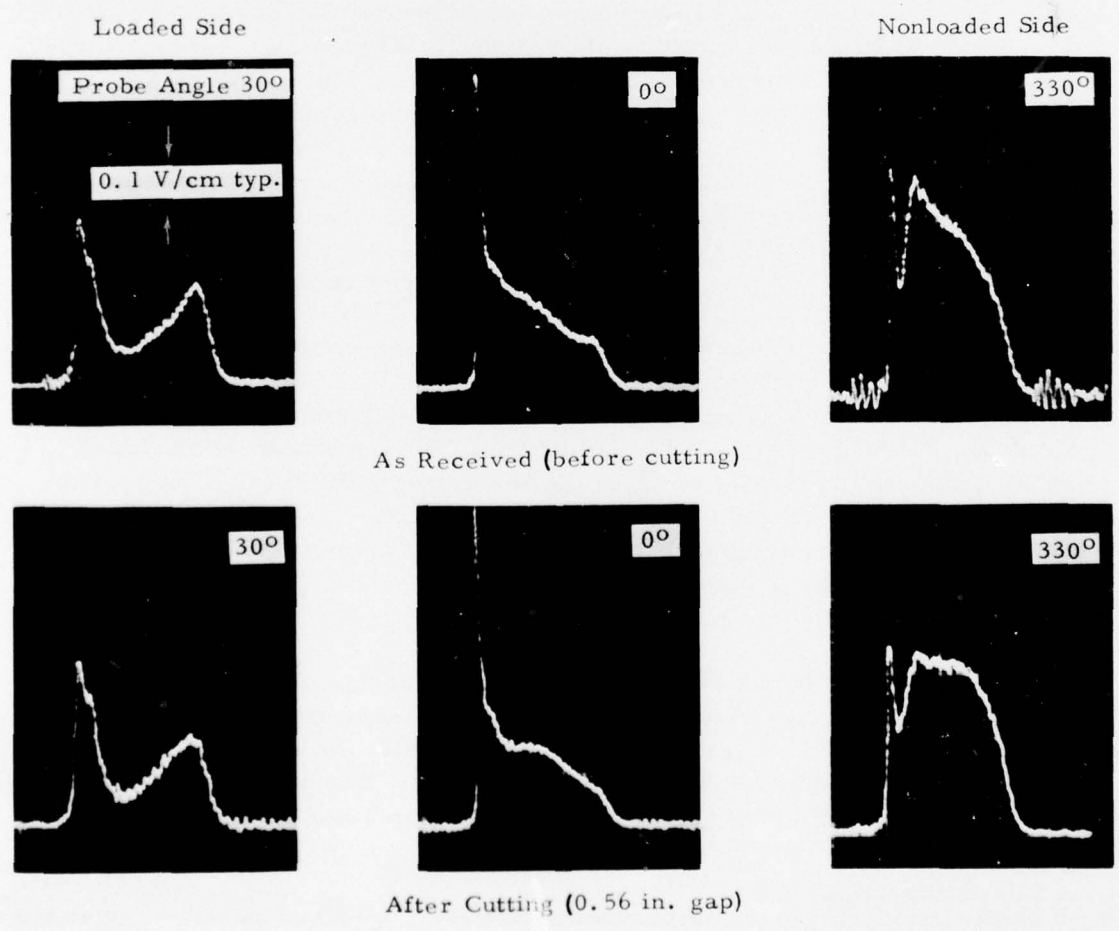


FIGURE 3A. BARKHAUSEN NOISE SIGNATURES BEFORE AND AFTER CUTTING A FAILED J85 MAIN BEARING (S/N 2416)

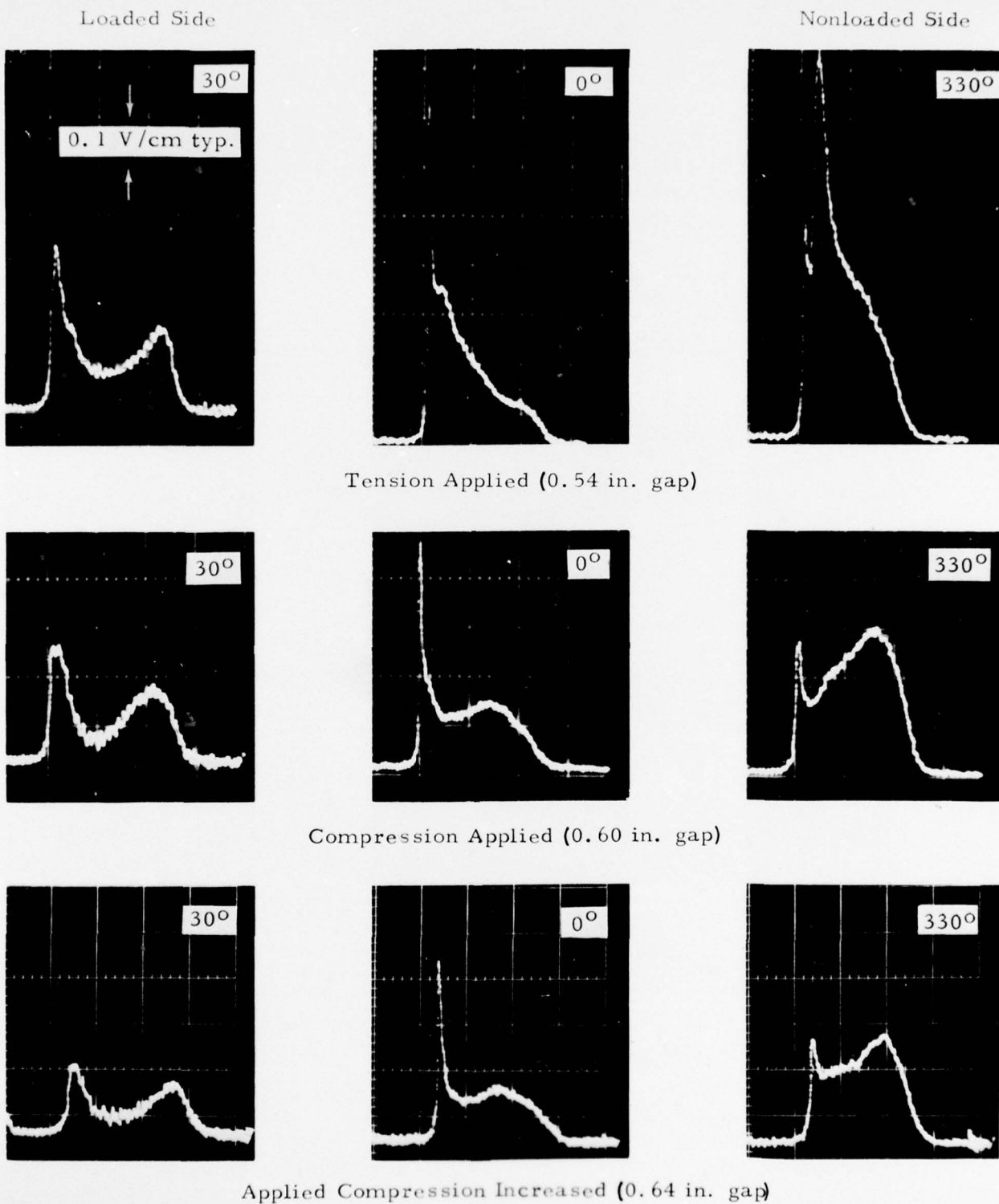


FIGURE 3B. BARKHAUSEN NOISE SIGNATURES WITH TENSION AND COMPRESSION APPLIED AFTER CUTTING A FAILED J85 BEARING (S/N 2416)

Christi Army Depot (CCAD), and in some instances is referred to as the prototype (CCAD) unit. In this report, both the preliminary prototype unit and the prototype inspection system are described including verification test results. Metallurgical sectioning results confirming flaw detection capabilities are included. Related inspection results from refurbished main shaft and transmission bearings (UH-1 helicopter) using magnetic perturbation, Barkhausen, and laser scattered light inspections, conducted using laboratory equipment, have been reported elsewhere. (2)

Items delivered under the subject contracts include the following:

- (1) Prototype bearing inspection system (15-3764-078)
- (2) Drawings for prototype inspection system
- (3) Specifications for bearing inspection system
(Document Number SwRI 3764-DOC-1 Rev A)
- (4) Operating Instruction Manual.

A general description of the bearing inspection system and a summary of capabilities are presented in this report. A more detailed discussion of the equipment has been presented in the Operating Instruction Manual, Drawings and Specifications.

II. PROTOTYPE INSPECTION SYSTEM

A. Description

The bearing inspection system, illustrated in Figure 4, employs magnetic perturbation and Barkhausen noise methods to inspect antifriction bearing race elements for surface and subsurface inclusions, indents, microcracks, spalls, and detrimental changes in residual stress, etc. The inspection system is semiautomatic; an operator performs such functions as mounting fixtures to accommodate the different bearing elements to be inspected and interfacing with a supervisory control computer. The computer acts in response to operator instructions and automatically controls and monitors inspection sequences. Data from all inspections are recorded on analog magnetic tape; simultaneously "threshold level" detection* signal analysis is performed automatically and the type and location (azimuthal and transverse) of all signals, which exceed the threshold level, are printed out in hard copy on a teleprinter.

The control console is illustrated in Figure 5 where several major subsystem items are identified. A master supervisory control program is stored in the computer by "reading it in" from a punched paper tape via the tape reader. Inspection parameters for each type of bearing element are automatically set up by reading the values in from a parameter tape (hereafter called a P-tape) via the tape reader at the request of the supervisory program. Communication between the computer and the operator is carried out via a teleprinter.

A closeup view of the race inspection unit is shown in Figure 6. In this view the cover on the inspection unit has been opened and a microscope (with camera) is mounted for visual correlation examination. During a routine inspection sequence, the microscope is not mounted and the cover is closed to maintain a clean atmosphere at slight "positive" pressure in the cabinet and to provide safety for the operator. Inspection of different element types is accommodated by changing specific fixtures or accessories; the pole pieces (including Barkhausen and magnetic perturbation mechanisms) and the chuck jaw assembly, shown in Figure 6, comprise the accessory pieces.

The functional block diagram of the bearing race inspection system, shown in Figure 7, illustrates the mechanical, electromechanical,

* The term "threshold level" detection refers to a simple signal detection approach wherein a signal is "recognized" when it has an amplitude which exceeds a preset voltage (threshold amplitude or level).

3626

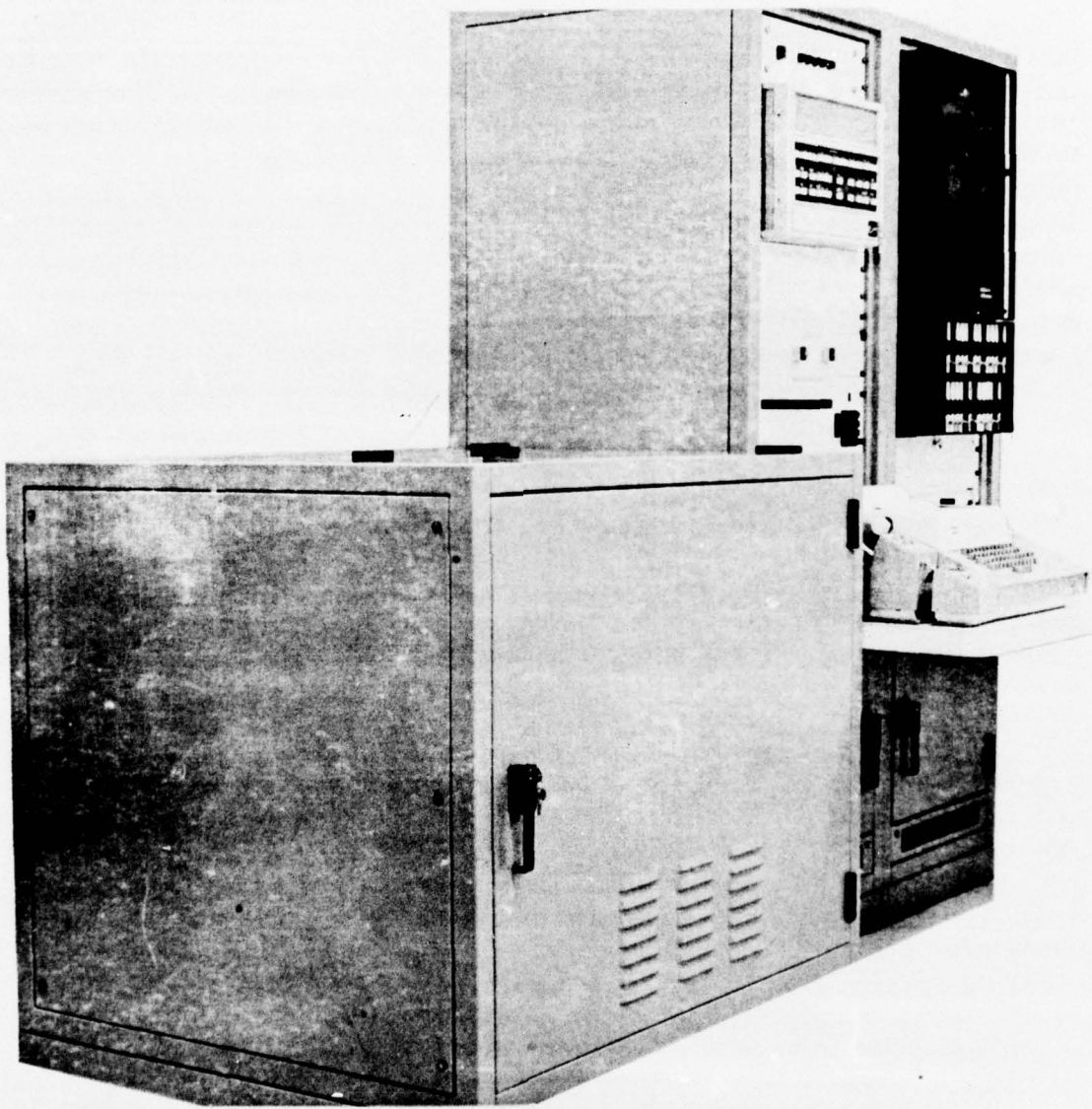


FIGURE 4. BEARING INSPECTION SYSTEM

3628

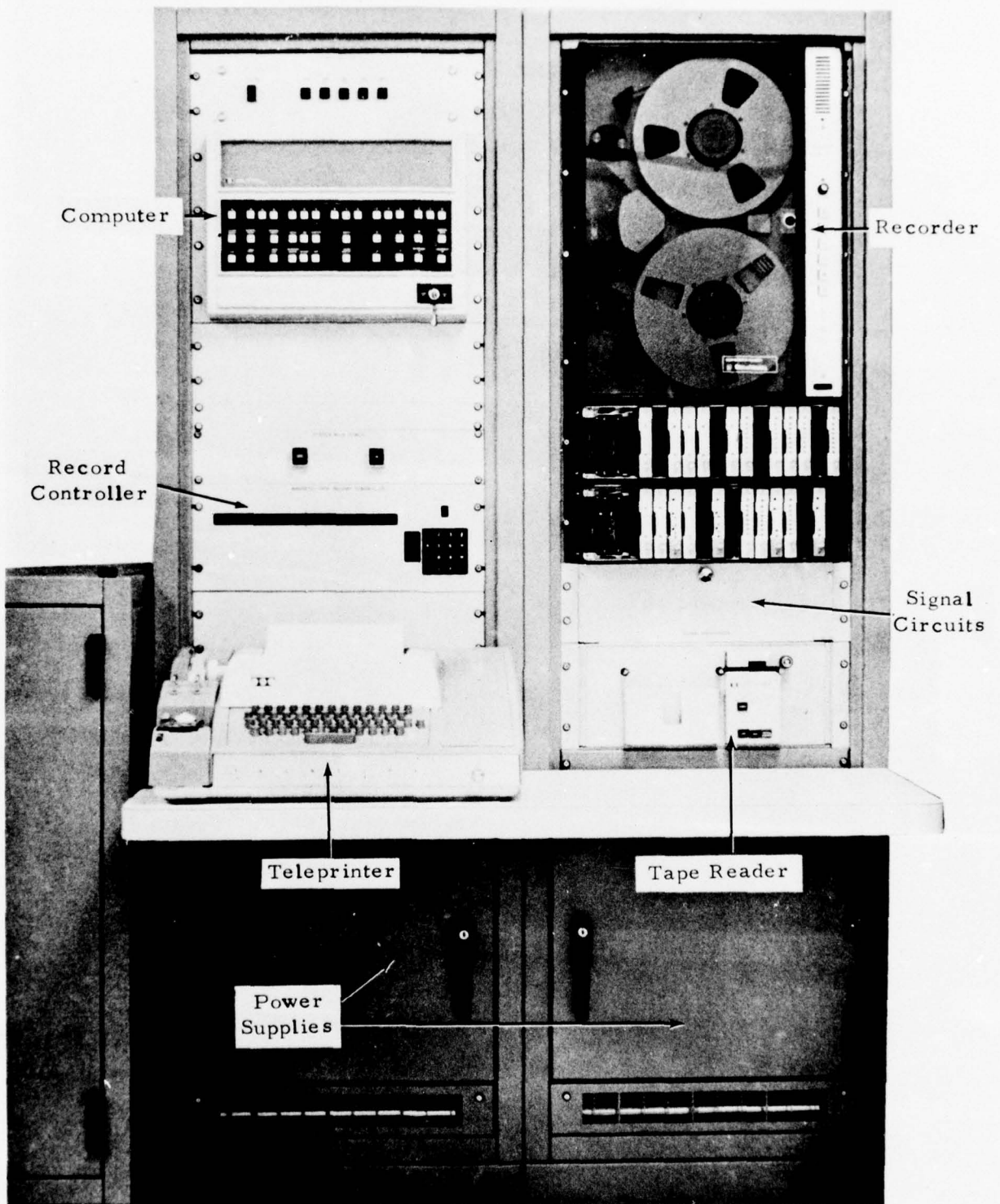


FIGURE 5. CONTROL CONSOLE

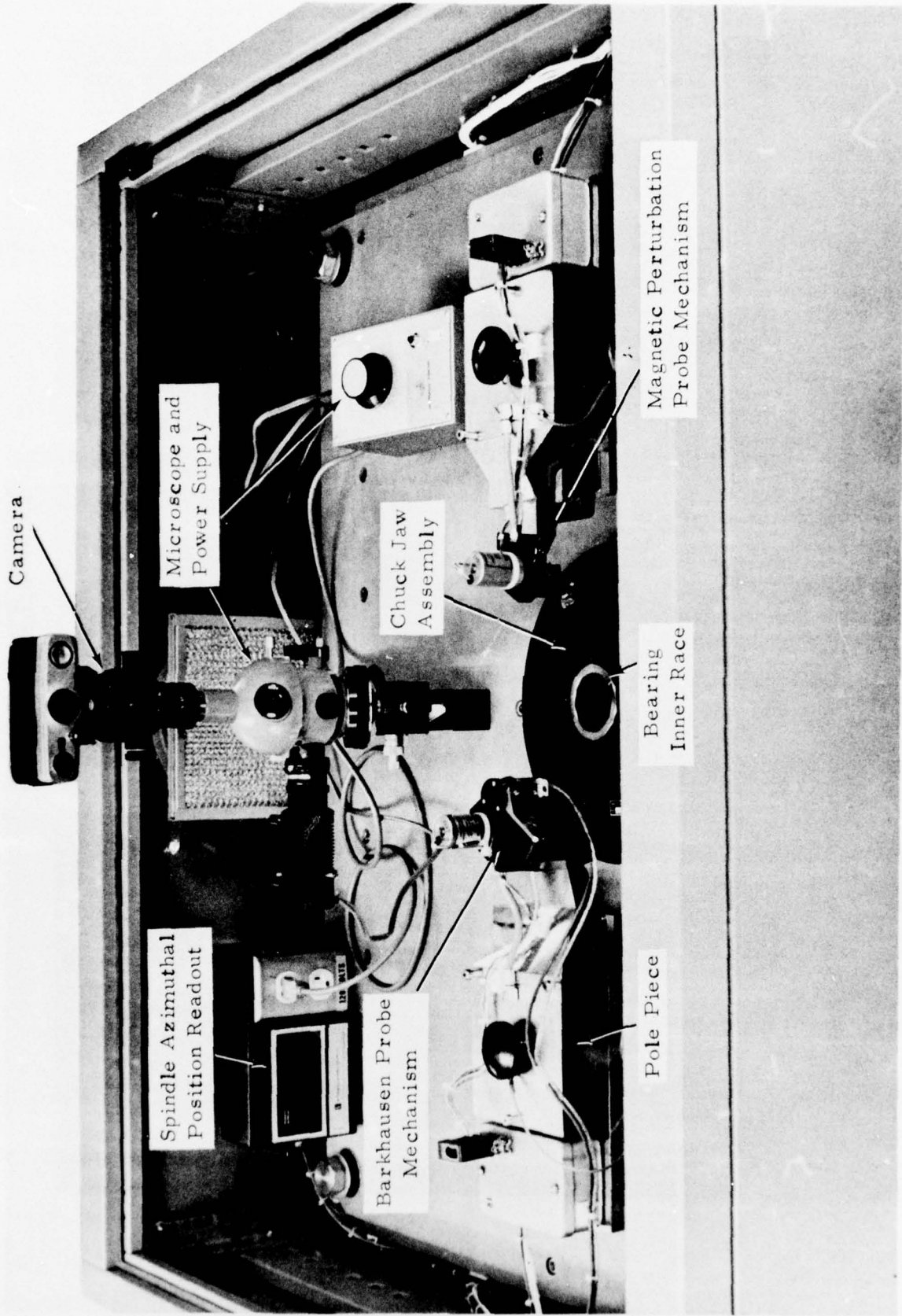


FIGURE 6. RACE INSPECTION UNIT

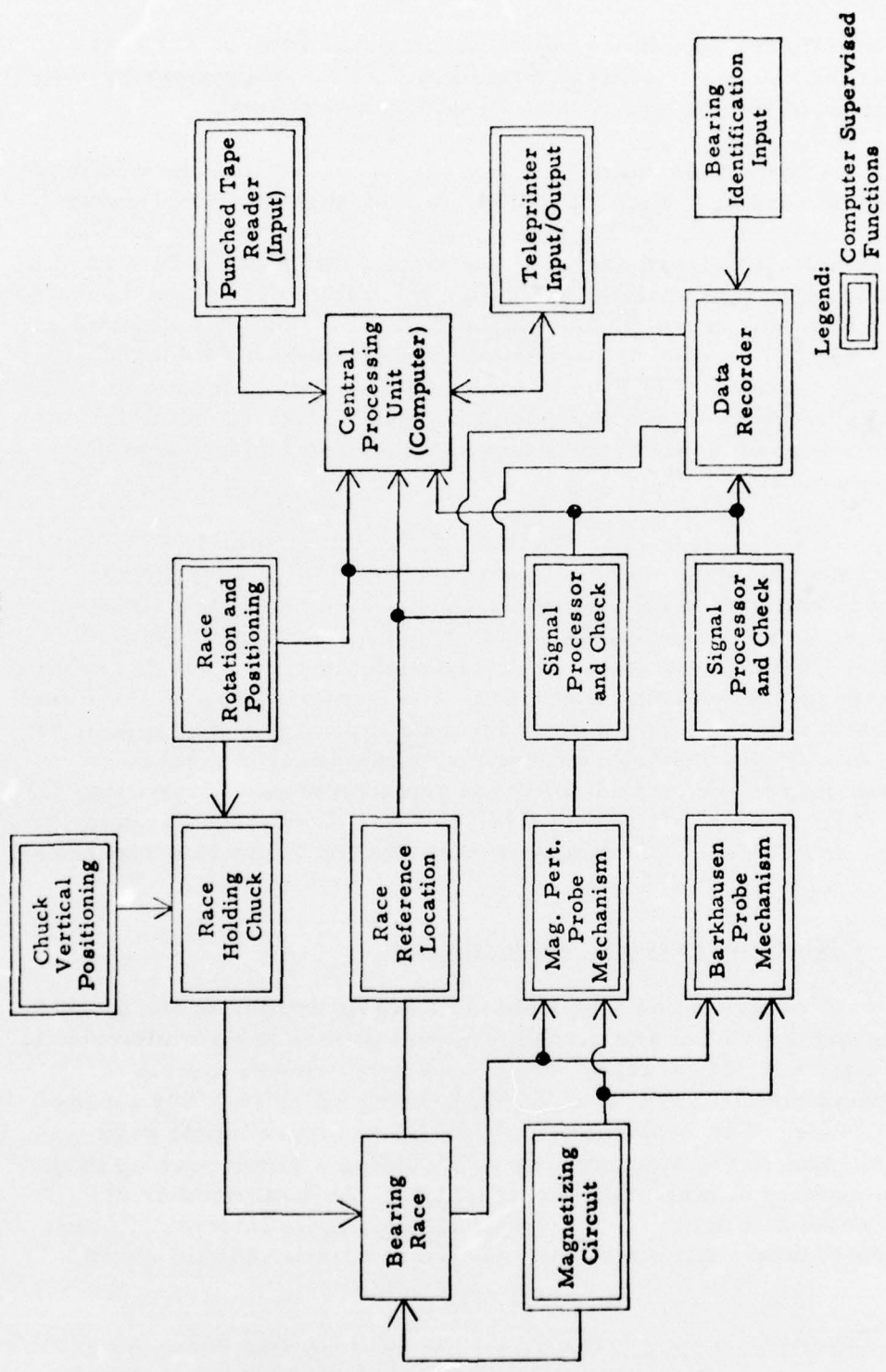


FIGURE 7. FUNCTIONAL DIAGRAM OF BEARING RACE INSPECTION SYSTEM

and electronic functions performed under computer control and supervision including holding, rotating, and magnetization of the bearing race and acquisition of the signatures and signature location data.

A brief description of a typical inspection sequence follows; referral by the reader to Figures 4 through 7 throughout the following description is suggested. The operator enters descriptive information, via the teleprinter keyboard, about the bearing component to be inspected. Based on this input information, the computer prints out for the operator the specific fixturing (race chuck, magnetizing and sensing elements) to be mounted and the inspection parameter tape (P-tape) to be loaded via the paper tape reader. The P-tape enters into the computer memory the necessary parameters to accomplish an automatic inspection on the specified bearing component, and essentially all remaining inspection steps are automatic.

The operator is instructed via the teleprinter to load the bearing component, and close the loading access door. Subsequently, the bearing is clamped via a pneumatic chuck, the spindle is raised to the inspect position, air is turned on to produce air coupling between the probes and the bearing component, and the pole pieces are brought into proximity to the bearing race. The race is rotated at a programmed speed to obtain a surface speed of 90 inches per second. The reference line on the face of the bearing is sensed with an optical pick-up head; the computer stores the location of the bearing reference mark with respect to the spindle shaft-encoder reference. When the reference line location is acquired, the magnetic perturbation inspection sequence proceeds.

Magnetic Perturbation Inspection

A programmed high field current* is applied to the magnetizing coils and the radial and circumferential probes are simultaneously indexed to adjacent scan tracks. Each scan track covers a strip of surface around the circumference of the bearing which is 0.025 inches (0.625 mm) wide. The probes are indexed by a stepper motor 0.02 inches (0.50 mm) to the adjacent track, providing a slight overlap in the scan. The number of steps between tracks and the total number of tracks inspected are supervised by the computer from information contained in the P-tape. Each track is scanned for three revolutions; the

* Performing the high field inspection first assures that the prior unknown magnetic history of the specimen does not randomly influence inspection results.

signal data from which are recorded on an analog magnetic tape recorder. The scan track and azimuthal locations of signals exceeding a preset threshold level are stored in the computer (in a buffer memory) for later printout. On completion of all track locations at high magnetic field, the radial and circumferential probes are automatically returned to "track zero". The magnetizing field is decreased to a preprogrammed low field current, the probe scan tracks are repeated, and the data are recorded on magnetic tape. Locations of signals exceeding a threshold at low field are also stored in the computer. The magnetic perturbation probes are returned to track zero, the magnetizing current is programmed to zero, spindle rotation is programmed to zero, and the type (radial or circumferential and high or low field) and location of signals exceeding the preset threshold levels are printed out. The operator is instructed to reduce the selected magnetic tape transport speed for the subsequent Barkhausen noise inspection.

Barkhausen Noise Inspection

The bearing is slowly rotated automatically, until the Barkhausen probe is in alignment with the reference mark on the bearing, the magnetizing power supplies are reconfigured so that a controlled, time-varying current is applied to the magnetizing coils. Barkhausen signatures are recorded and monitored for three successive magnetization cycles at each of three transverse probe locations. Subsequently, this inspection sequence is repeated at azimuthal positions 120° and 240° from the initial position, respectively. The operator is then instructed to increase the selected tape transport speed.

Demagnetization

The bearing component is then automatically demagnetized by: reconfiguring the magnetizing power supplies, applying high field followed by programming the field to zero while the bearing is rotating rapidly, subsequently withdrawing the pole pieces, and lowering the spindle. Subsequent to demagnetization, the location of signals exceeding the preset threshold criteria for the Barkhausen noise inspection are printed out.

Other Inspection Mode Options

Upon completion of the automatic inspection sequence on a bearing from which "flaw" printouts are obtained, the operator is given several options; a) to conduct a visual inspection, b) to repeat any one or more of the inspections in a manual mode, c) to rerun the automatic mode for either or both types of inspections. A visual inspection is

facilitated using the spindle azimuthal position readout (see Figure 6) and positioning micrometers on the microscope assembly in conjunction with the signal or "flaw" printout.

B. Capabilities

The bearing inspection system provides for the inspection of ball and roller bearing inner and outer race elements using magnetic perturbation and Barkhausen noise methods. The basic system is designed to inspect bearing elements in the following size ranges:

Races:	I. D.	=	1.90" (4.83 cm) min.
	O. D.	=	10.0" (25.4 cm) max.
	Width	=	0.2" - 2.0" (0.51 cm - 5.1 cm)

Within this size range specific fixtures are supplied to inspect the bearing elements given in Table I. In addition, designs have been completed for the other bearing races indicated in Table II; these fixtures were not fabricated.

A typical set of fixturing is illustrated in Figure 8 and consists of a set of chuck jaws and pole piece-probe mechanism assemblies for the inner race and another set for the outer race. The fixturing set also includes an inner and outer race with a small machined hole and an indent as reference flaws; these components provide a permanent reference for checking system inspection consistency.

The features and specifications of the bearing inspection system are summarized in Figure 9. The system developed and delivered under the subject contracts incorporates all inspection methods specified in Figure 9, except laser-scattered light; however, the delivered system can be expanded to include the scattered light inspection.

TABLE I

BEARING INSPECTION ACCESSORIES COMPLETED

Bearing, Inspection Fixture, and P-Tape Code Identification

<u>Bearing Assembly</u>			<u>Bearing Component, Fixture & P-Tape Code ID</u>	
<u>Eng/Trans.</u>	<u>Military P/N</u>	<u>Code ID</u>	<u>Inner Race</u>	<u>Outer Race</u>
T53	1-300-015	00	000	004
T53	1-300-176-02/03	01	010	014
T53	1-300-176-01/04	02	020	024
UH-1	204-040-346	07	070	074
UH-1	205-040-246	09	090	094

TABLE II

BEARING INSPECTION ACCESSORY DESIGNS COMPLETED

<u>Eng/Trans.</u>	<u>Military P/N</u>	<u>Code ID</u>
T55	2-300-001	03
	2-300-011	04
	2-300-035	05
UH-1	204-040-270	06
	205-040-245	08

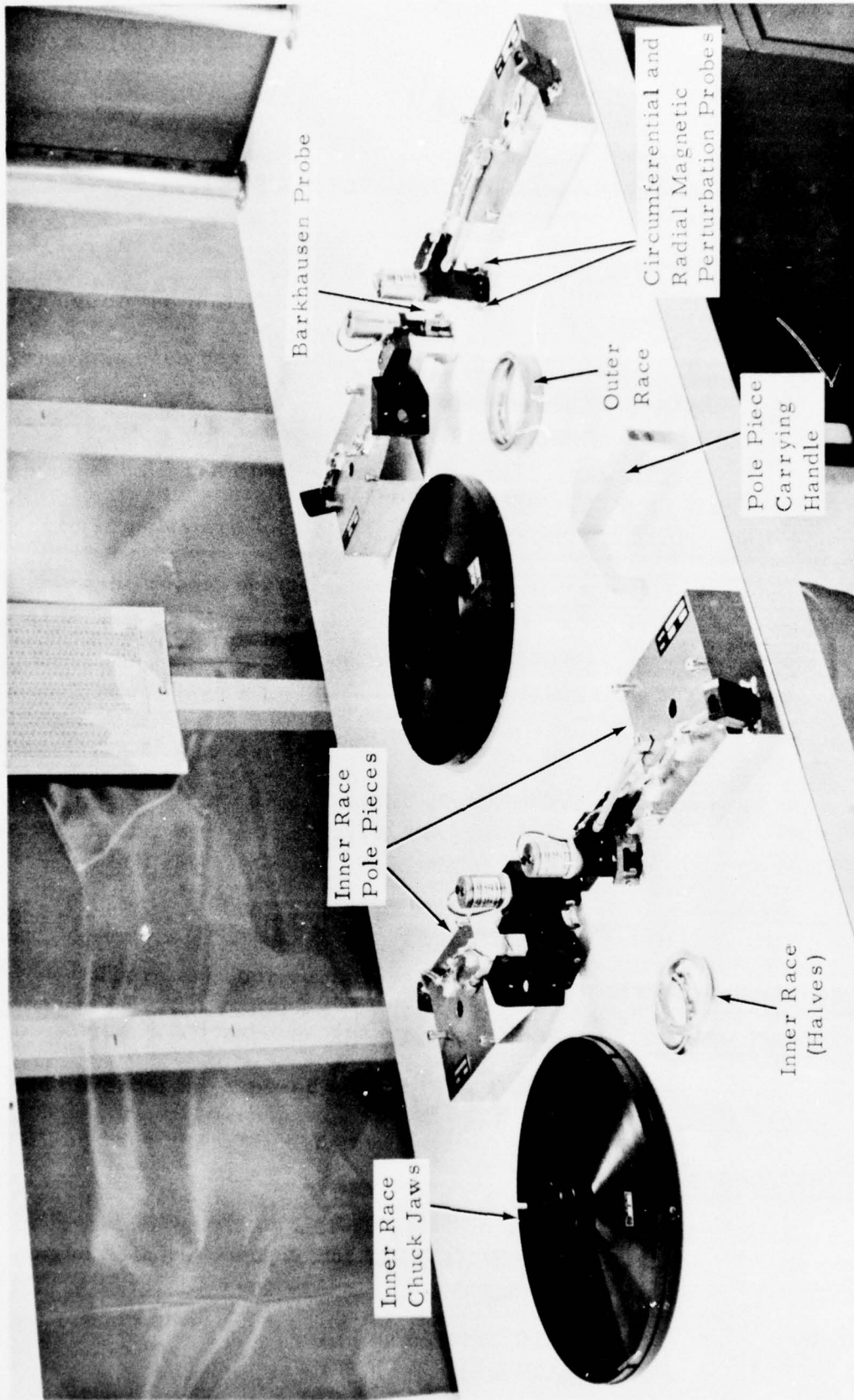


FIGURE 8. TYPICAL RACE ELEMENT INSPECTION FIXTURES

CIBLE

(Critical Inspection on Bearings for Life Extension)

AUTOMATED BEARING INSPECTION SYSTEM

FEATURES

- COMPUTER SUPERVISED AND CONTROLLED INSPECTION
- RAPID FIXTURING CHANGEOVER FOR DIFFERENT BEARINGS
- COMPUTER SETUP OF PARAMETERS FOR DIFFERENT BEARINGS
- COMPUTER PRINTOUT OF SIGNAL LOCATIONS
- PERMANENT RECORD ON MAGNETIC TAPE
- DIAGNOSTIC PRINTOUTS AND SAFETY INTERLOCKS

SPECIFICATIONS

INSPECTION METHODS	CONDITIONS DETECTABLE	SCAN PATTERN
<u>MAGNETIC PERTURBATION</u>		
<u>RADIAL FLUX</u>		
● HIGH FIELD	SURFACE PITS, INCLUSIONS, SPALLS AND INDENTATIONS	0.025-INCH WIDE CIRCUMFERENTIAL STRIPS WITH 20% OVERLAP
● LOW FIELD		
<u>CIRCUMFERENTIAL FLUX</u>		
● HIGH FIELD	SUBSURFACE INCLUSIONS, AND SPALLS AND DEEPER SURFACE ANOMALIES	12 TO 60 SCANS PER INSPECTION METHOD
● LOW FIELD	FATIGUE DAMAGED REGIONS AND INDENTATIONS	
<u>LASER-SCATTERED LIGHT</u>		
<u>SURFACE ANOMALY</u>	SURFACE SCRATCHES, PITS, SPALLS, AND INDENTATIONS	SYNCHRONIZED SCANS
<u>SURFACE FINISH</u>	RELATIVE SURFACE FINISH	
<u>BARKHAUSEN NOISE</u>		
	RELATIVE SURFACE AND NEAR-SURFACE RESIDUAL STRESS CONDITIONS	PROGRAMMED SAMPLING 0.050 × 0.050- INCH REGIONS 9 TO 15 LOCATIONS
	SERVICE MODIFICATION OF RESIDUAL STRESS	

FIGURE 9. SUMMARY OF CIBLE BEARING INSPECTION SYSTEM FEATURES AND SPECIFICATIONS

III. INSPECTION DATA AND RESULTS

Typical printouts and signatures, verification test and verification cross-check results are presented in this section.

A. Verification Cross-Check

Control reference inner and outer bearing races, containing manufactured defects, were inspected on both the preliminary prototype unit and prototype system to determine the degree of correlation between inspection results. Typical printouts for the two systems are illustrated in Figure 10. A brief explanation of the printouts follows.

Note in Figure 10 that the printout of magnetic perturbation "flaw" signals is preceded by instructions to the operator regarding entry of bearing descriptive and service data. The printout for magnetic perturbation, near the top of Figure 10, from left to right gives:

- a) the type of inspection (TY) where R = radial, C = circumferential, H = high field, L - low field;
- b) transverse position of the probe (P ST) in the number of steps from Track zero;
- c) azimuthal location of signal from reference line on the bearing (B R) where 2500 corresponds to 180° and 5000 is one complete revolution or 360°; and
- d) azimuthal signal location with respect to the spindle shaft encoder zero (S R). *

Immediately preceding the flaw printout data, a printout is given for: a) the location of the shaft zero when the bearing reference line is detected, and b) the location of the bearing reference line with respect to the shaft zero. A similar printout is shown for the Barkhausen and laser inspections also; however, no Barkhausen flaw signals were detected. A comparison of the printouts in Figure 10 for the preliminary and prototype units shows there is excellent agreement between the two

* Spindle reference position readout is displayed on the spindle azimuthal position readout (See Figure 6). It facilitates positioning of the bearing for microscopic examination of the race surface at physical locations corresponding to flaw printout locations.

units for type, scan track, and azimuthal position. For reference, one count in BR or SR is equivalent to ~ 0.001 inch (0.025 mm).

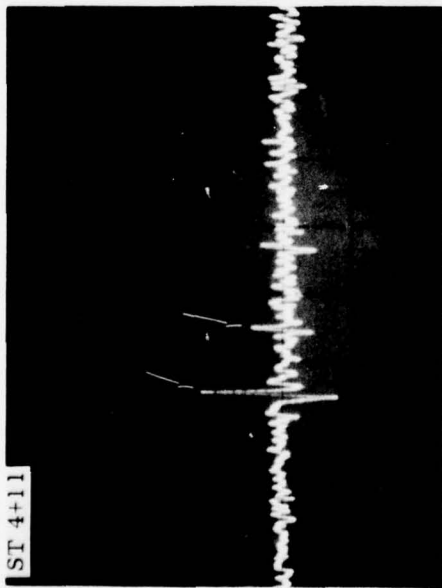
A more critical cross-check consists of comparing the analog signatures from manufactured flaws for the two units. Figure 11 shows a comparison between the magnetic perturbation circumferential and radial high field signatures from the same inner race half. The signals pointed out by the arrows in each record are from a 0.007 inch diameter x 0.004 inch deep (0.175 x 0.1 mm) indent and a 0.007 inch diameter x 0.002 inch deep (0.175 x 0.05 mm) lapped hole left to right, respectively, in each case. A direct comparison between signatures from the two units is possible by examination of the records in the upper and lower rows, respectively, in Figure 11. Amplitude agreement is within $\pm 10\%$ and detailed signal content correlation is excellent; data presented are for the same scan track location.

Figure 12 presents comparative results for Barkhausen signatures. A brief discussion of these results is appropriate because of certain unusual signature characteristics. Although the Barkhausen signatures for both units are essentially identical (see left column of records, Figure 12), certain nonvalid signature characteristics are pointed out by the arrows. The occurrence of such nonvalid signatures was suspected during setup and checkout of accessories for 204-040-346/205-040-246 inner races on the prototype system before delivery. Delivery of this accessory set was temporarily withheld pending further investigations. It was determined subsequently, that vibration-induced extraneous signal was present (see discussion of vibration-induced signal in Appendix). The signature at the right in Figure 12 illustrates the valid signature subsequent to elimination of the problem; note the absence of the "humps" present in the signatures at the left in Figure 12.

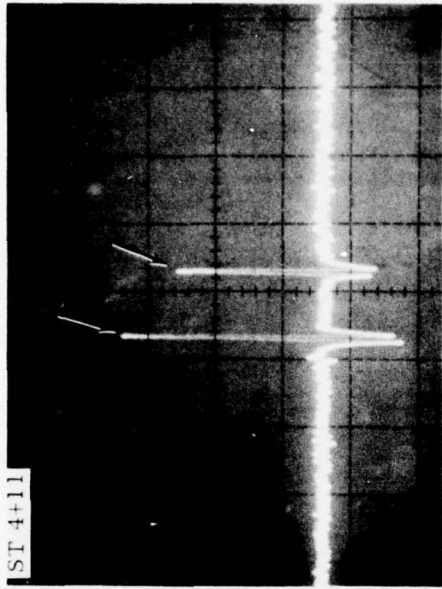
Figures 13 and 14 illustrate comparative magnetic perturbation and Barkhausen signatures, respectively, from manufactured flaws in a control reference outer race element. Signal amplitude agreement is within $\pm 15\%$ with excellent signal content correlation. No extraneous signal is present in the Barkhausen signatures (see Figure 14).

B. Refurbished Bearing Inspection (Using Laboratory Apparatus)

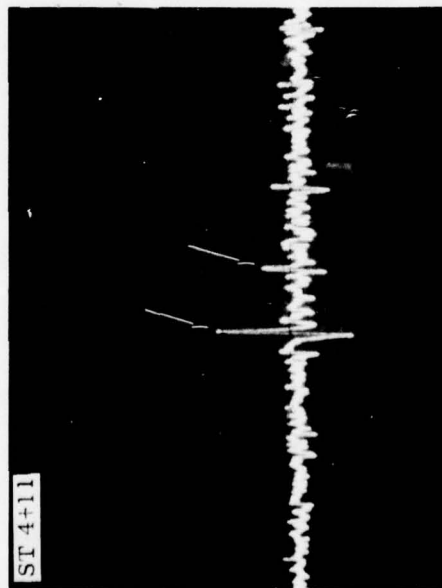
During the early stages of preliminary prototype development, qualification of a relatively extensive procedure to refurbish helicopter engine and transmission bearings, which included regrinding of the raceways and retrofitting with larger matching rolling elements, was undertaken by the Army. It was decided to include the new NDE methodology being developed under the CIBLE program. Laboratory setups (see



Prototype (CCAD) System

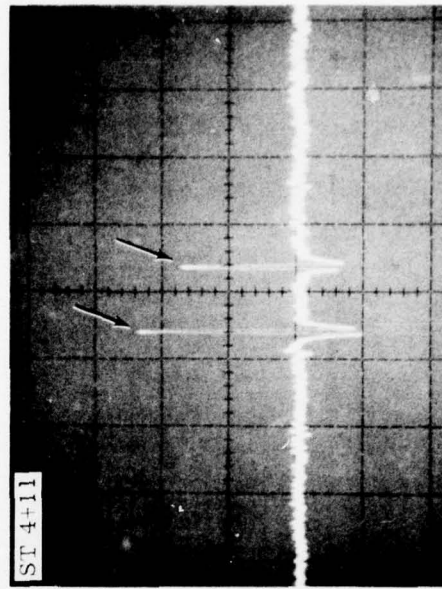


Prototype (CCAD) System



Preliminary Prototype Unit

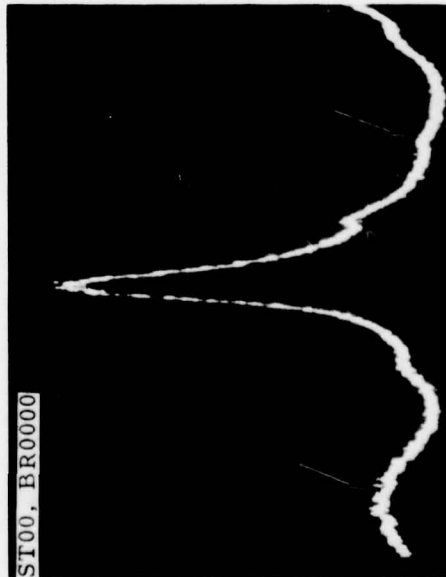
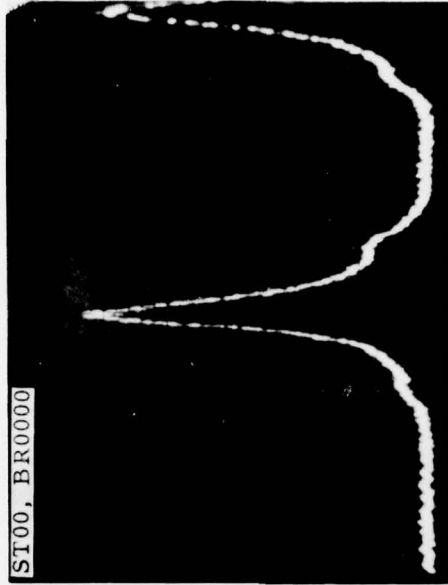
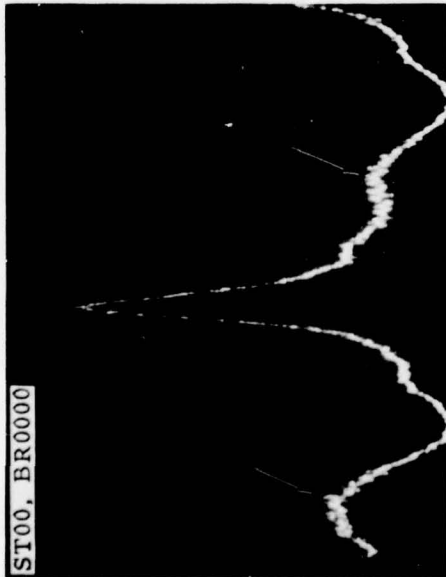
Circumferential
Vertical Sensitivity 0.5 V/div
Horizontal Sweep 1 msec/div



Preliminary Prototype Unit

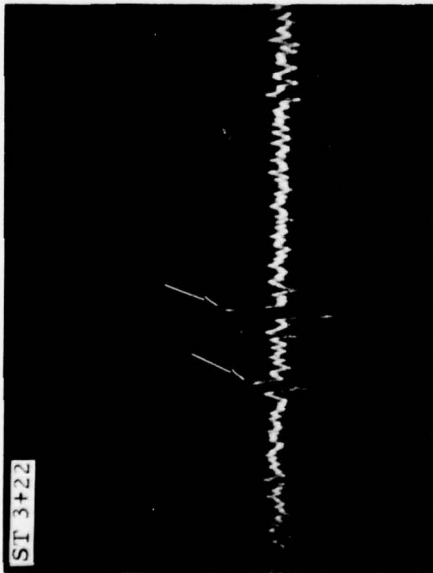
Radial
Vertical Sensitivity 0.5 V/div
Horizontal Sweep 1 msec/div

FIGURE 11. COMPARISON OF PROTOTYPE (CCAD) AND PRELIMINARY PROTOTYPE UNIT MAGNETIC PERTURBATION SIGNATURES FROM MANUFACTURED DEFECTS IN SAME INNER RACE (PN 1-300-015, S/N 759P)



Vertical Sensitivity 50 mV/div
Horizontal Sweep 0.2 sec/div

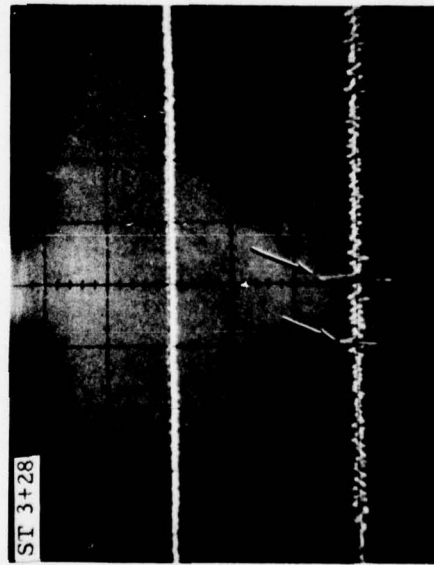
FIGURE 12. COMPARISON OF PROTOTYPE (CCAD) AND PRELIMINARY PROTOTYPE UNIT BARK-HAUSEN SIGNATURES FROM SAME INNER RACE (PN 1-300-015, S/N 759P) (Before and After Elimination of Air Induced Vibration Signal)



Prototype (CCAD) System

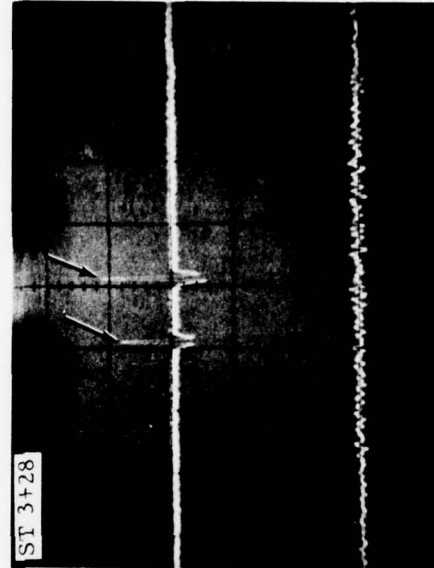


Prototype (CCAD) System



Preliminary Prototype Unit
Circumferential

Vertical Sensitivity 0.5 V/div
Horizontal Sweep 1 msec/div

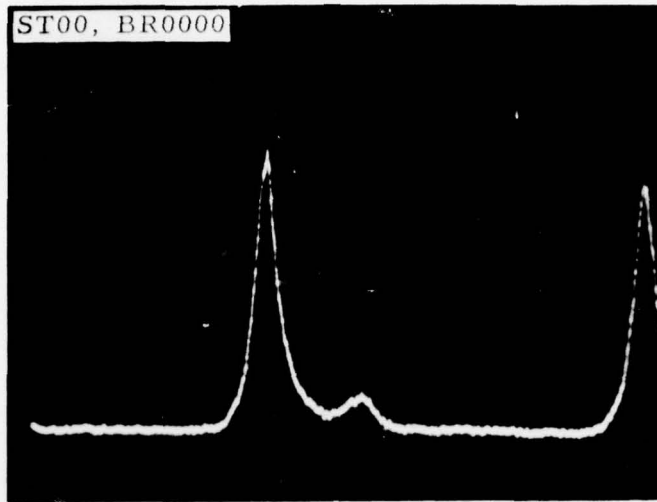


Preliminary Prototype Unit
Radial

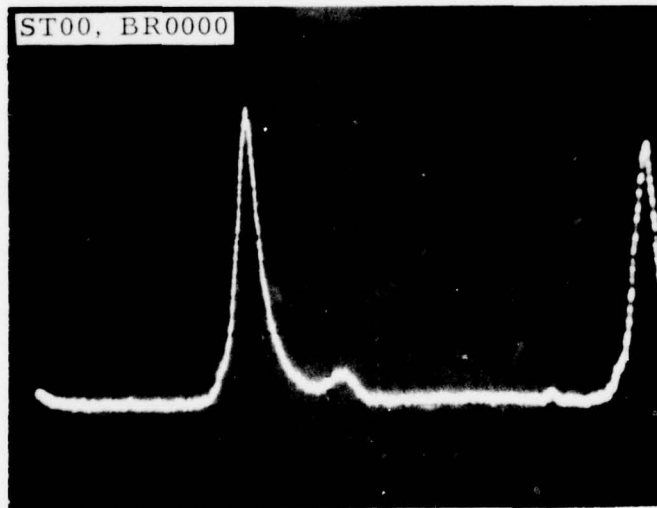
Vertical Sensitivity 0.5 V/div
Horizontal Sweep 1 msec/div

FIGURE 13. COMPARISON OF PROTOTYPE (CCAD) AND PRELIMINARY PROTOTYPE UNIT MAGNETIC PERTURBATION SIGNATURES FROM MANUFACTURED DEFECTS IN SAME OUTER RACE (PN 1-300-015, S/N 759P)

3976



Prototype (CCAD) System



Preliminary Prototype Unit

Vertical Sensitivity 0.1 V/div
Horizontal Sweep 0.2 sec/div

FIGURE 14. COMPARISON OF PROTOTYPE (CCAD) AND PRELIMINARY PROTOTYPE UNIT BARKHAUSEN SIGNATURES FROM SAME OUTER RACE (PN 1-300-015, S/N 759P)

Figures 15 and 16) were adapted to facilitate the acquisition of magnetic perturbation, Barkhausen noise, and scattered light inspection data on a group of the refurbished bearings prior to physical testing of the bearings. The inspection results obtained have been reported previously⁽²⁾ and only a brief summary will be presented here.

The apparatus used for magnetic perturbation inspection of bearing races is illustrated in Figure 15. This apparatus facilitated the acquisition of magnetic perturbation circumferential and Barkhausen noise data on both inner and outer races. The laboratory apparatus in Figure 16 was used to acquire laser scattered light data. Such inspections were conducted on 20 each reference Part Number 1-300-015-04 (ITI PN 13701), 20 each reference Part Number 1-300-176-03 (ITI PN 13700), engine main shaft bearings and 20 sets of 3 each reference Part Number 205-040-246-3 (ITI PN 13699) transmission bearings. Several magnetic perturbation signatures considered significant were selected for more careful study and correlation examination with the physical surface of the raceway; a number of these locations have been reported on previously. However, because of unusual observations associated with a selected signature region, subsequent laboratory follow-up work was undertaken. Figures 17, 18, and 19 illustrate the results of an investigation only recently completed of this unusual region. In the upper record of Figure 17 the signal of interest is pointed out by the arrow; the lower record shows the same signature but with the horizontal scale expanded. This circumferential signature is well-shaped, with good symmetry (equally downward going and upward going peaks), and has void polarity indicative of a pit, hole or nonmetallic inclusion probably at or near the raceway surface. Both optical and scanning electron microscope (SEM) micrographs of the raceway region corresponding to the signal are presented in Figure 18. The very regular and uniform nature of the enclosing nearly perfect circular pattern generated intense interest in this region. Additional SEM examination at higher magnifications were undertaken of the region enclosed by the circular outline; regions marked A and B in the SEM micrograph at the bottom of Figure 18 are illustrated at higher magnification in Figure 19. The apparent cause of the magnetic perturbation signature is rust or corrosion and it is not superficial but probably extends 0.0005 to 0.0015 inches (0.013 to 0.038 mm) deep. The network of fine, crack-like lines in regions A and B (Figure 19) are apparently the result of oxide formation. This conclusion is supported by the X-ray fluorescence scan for oxygen in region B; note the dot pattern in the X-ray image of Figure 19 appears to correlate well with the visual elements of oxide evident in the SEM micrograph immediately to the left.

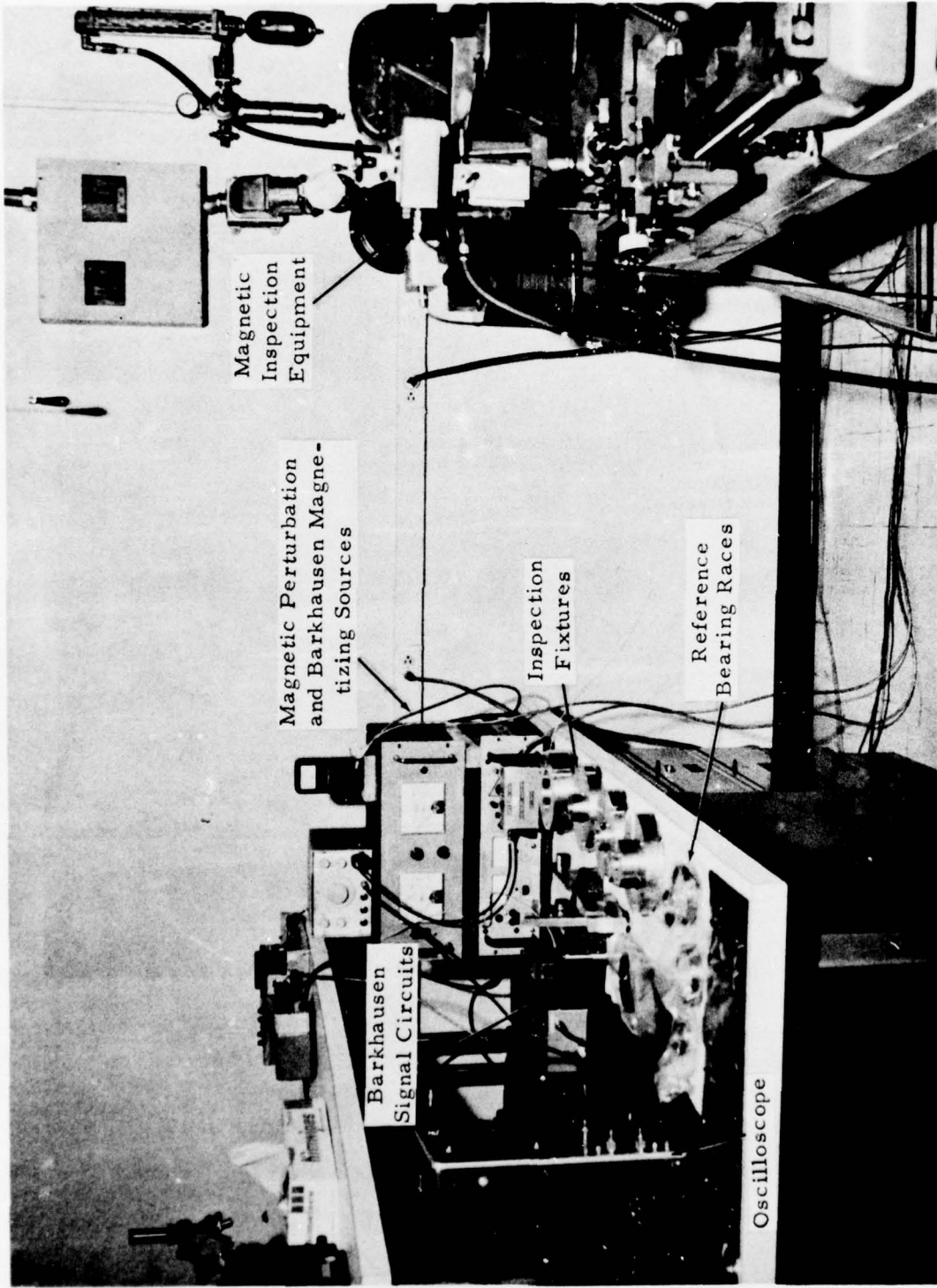


FIGURE 15. LABORATORY APPARATUS FOR MAGNETIC PERTURBATION AND BARKHAUSEN NOISE INSPECTIONS

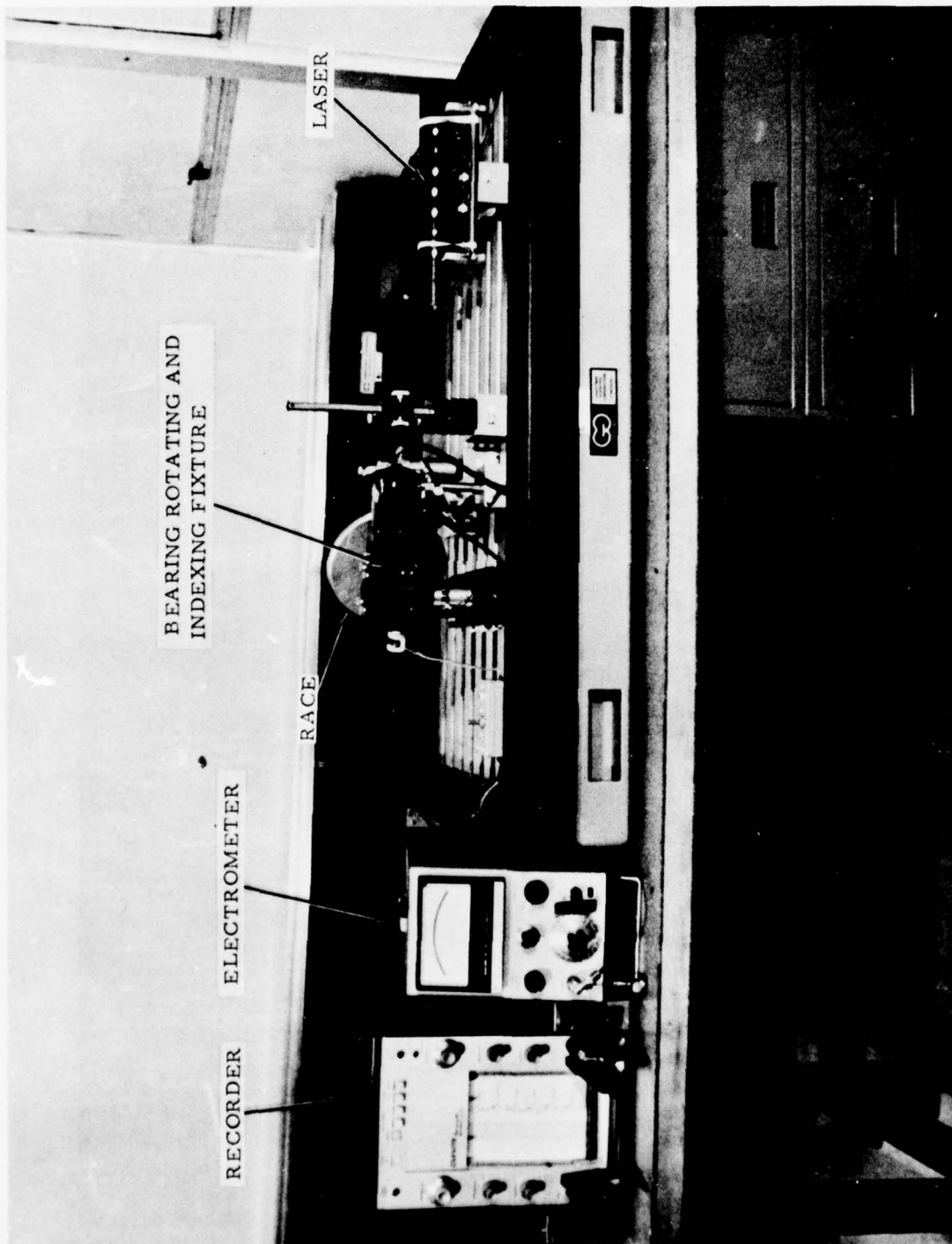
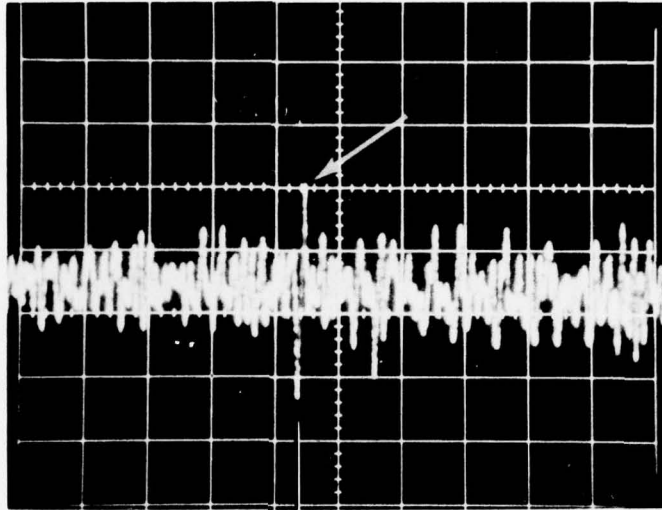
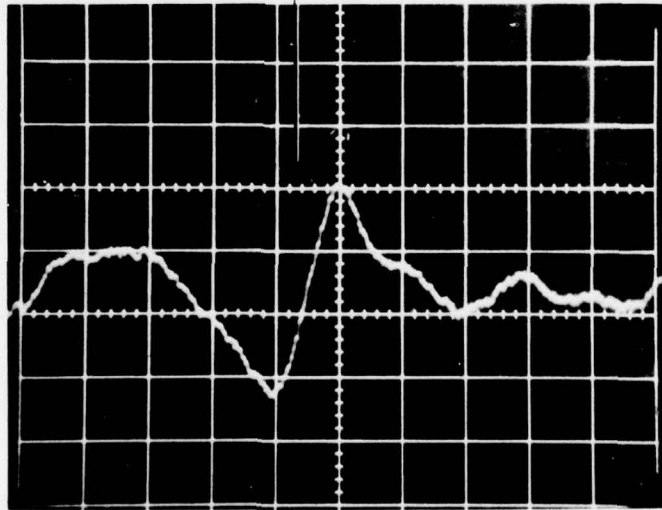


FIGURE 16. OVERALL VIEW OF OPTICAL INSPECTION SYSTEM

Vert. Sens. 20 mV/cm, Sweep 0.5 ms/cm



3785

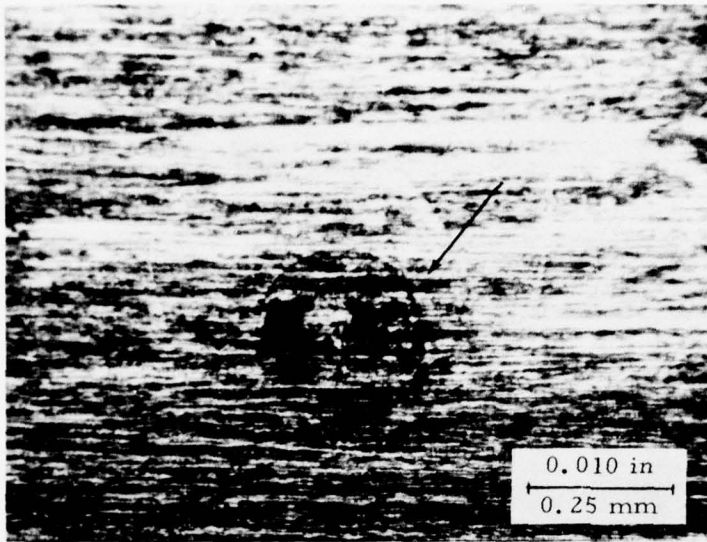


Vert. Sens. 20 mV/cm, Sweep 0.025 ms/cm

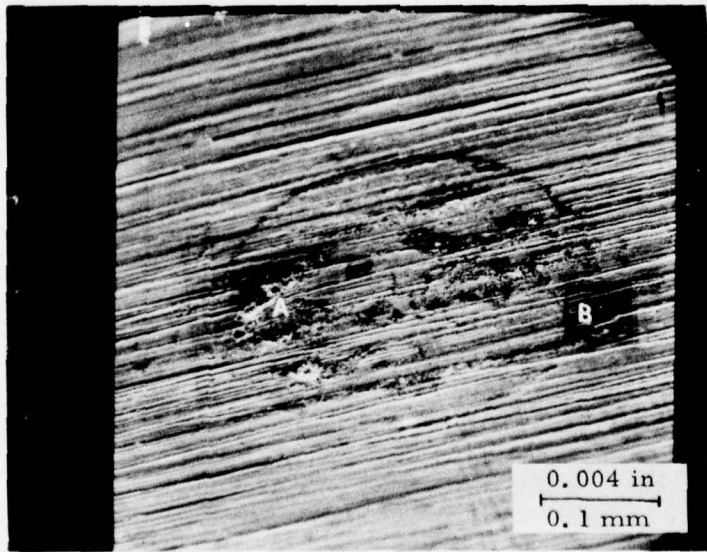
FIGURE 17. SELECTED MAGNETIC PERTURBATION CIRCUMFERENTIAL (High Field) RECORDS FROM A P/N 1-300-015, S/N 28, Side 2 (344°) REWORKED INNER RACE

P/N 1-300-015 Inner Bearing Race, Reworked
S/N 28, Side 2 (344°)

3786



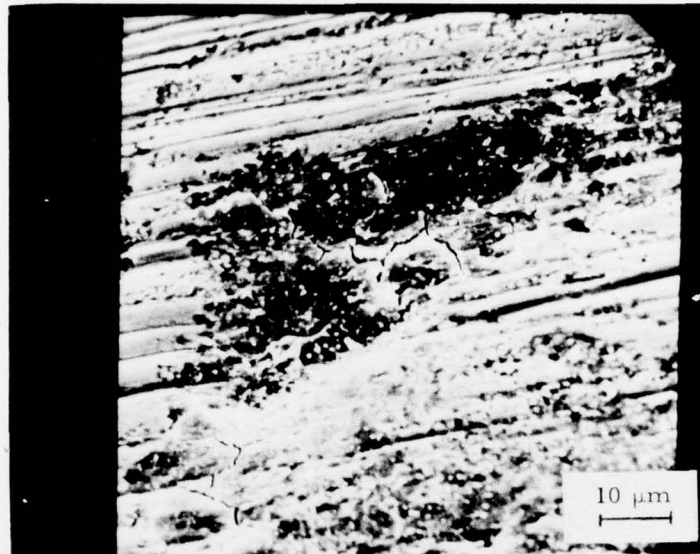
Optical Micrograph



SEM Micrograph

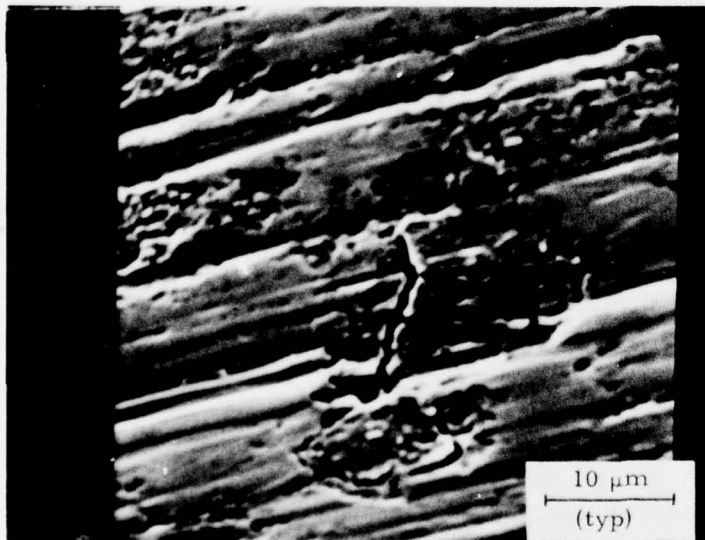
FIGURE 18. OPTICAL AND SEM MICROGRAPHS OF RACE SURFACE
CORRESPONDING TO MAGNETIC PERTURBATION CIR-
CUMFERENTIAL SIGNATURE

P/N 1-300-015, Inner Bearing Race, Reworked
S/N 28, Side 2 (344°)

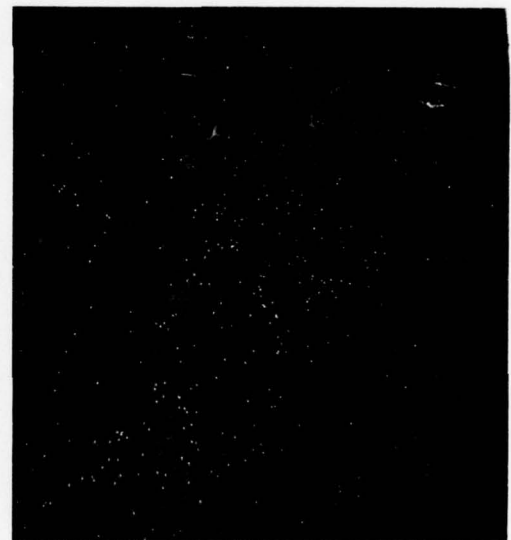


3787

SEM Micrograph Region A



SEM Micrograph Region B



X-Ray Image

FIGURE 19. SEM AND FLUORESCENCE MICROGRAPHS OF REGIONS A AND B

The results presented above, as well as those already published, establish the excellent sensitivity of the magnetic perturbation method to surface flaws; still other results to be presented in the sections which follow will establish the excellent sensitivity of the magnetic perturbation method to subsurface flaws and capability of the Barkhausen noise method for assessing the state of stress in the raceway.

C. Additional Bearing Inspection (Preliminary Prototype Unit)

As an effort under the subject program, a large number of bearing races were inspected, predominantly using the preliminary prototype unit at SwRI, as part of the verification tests. As a result of the inspection, a number of bearing races were selected for more comprehensive signature examination with emphasis on subsurface flaws and subsequent metallurgical sectioning. Initially, 480 used inner race pieces P/N I-300-015-04 were cleaned and visually examined to preclude possible damage to the magnetic perturbation and Barkhausen probes. The parts had been in bulk storage and severe indentations were observed in the edges of many of the inner races. Subsequently, 280 of these pieces were magnetically inspected. Flaw printouts were reviewed for those locations where magnetic perturbation circumferential printouts were obtained and yet no radial printouts coincided with these locations. The rationale of this approach follows:

- a) radial high field and also low field signatures usually are associated with shallow surface anomalies (indents) and deeper pits and inclusions which are open to the surface;
- b) circumferential high field signatures usually are associated with subsurface flaws and also with deeper and or larger surface anomalies;
- c) accordingly, a high field circumferential only printout indicates a signature from a possible subsurface inclusion site.

Table III summarizes the printouts obtained as a result of the inspection of 280 inner race pieces; a brief explanation of this table follows. Each piece is identified uniquely by serial number followed by a digit in parentheses which uniquely identifies each inner race half. The flaw printout results are tabulated based on the following: i) flaw printout from a given location obtained only for magnetic perturbation radial, ii) flaw printout for magnetic perturbation circumferential

TABLE III
SUMMARY OF INSPECTION FLAW PRINTOUTS
(P/N 1-300-015, Inner Races)

	<u>S/N</u>	<u>MPR (only)</u>	<u>MPC (only)</u>	<u>MPR & MPC</u>
1.	2079(0)	LF(1)	HF(1)	
2.	2298(0)		HF(1)	
3.	403AM(2)	HF & LF(1)		
4.	894V(2)	HF(1)		
5.	455Z(0)		HF(3)	
6.	455Z(2)	HF(1), HF & LF(1), LF(1)	HF(1)	
7.	171K(0)	HF(2), HF & LF(4)		
8.	171K(2)	HF(4), HF & LF(3), LF(1)		CH&RH&RL(1)
9.	4666(2)		HF(1)	
10.	165AF(0)			CH&RH&RL(1)
11.	108N(2)		HF(1)	
12.	652AA(2)		HF(1)	
13.	958AH(0)	HF & LF(3)		
14.	958AH(2)	HF & LF(1)		
15.	4930(2)	HF(1)		
16.	4270AS(2)	HF & LF(1)		
17.	458L(2)	HF(1)		
18.	230HH(2)	HF(1), HF & LF(1)		
19.	470V(2)		HF(2)	

Legend:

HF = high field
LF = low field

CH = circumferential high field
RH = radial high field
RL = radial low field

only, iii) flaw printout for magnetic perturbation radial and circumferential both at same location. In each case, the number of separate locations is indicated in parentheses following the designation of field level. For example, on line 7, bearing race S/N 171K(0) produced magnetic perturbation radial-only flaw printouts at two locations at high field, and four other locations at both high field and low field.

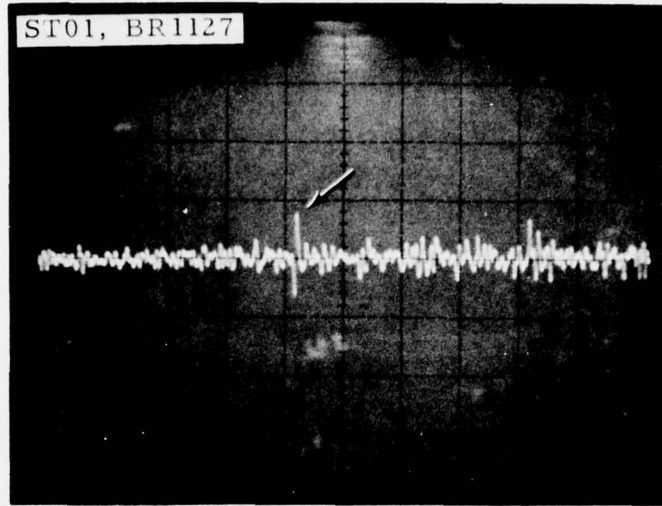
Examination of Table III in the magnetic perturbation circumferential-only column indicates that 8 pieces contained such signatures. The analog circumferential high field signatures on these bearing pieces were carefully examined and 3 of the pieces, 2079(0), 2298(0), and 470V(2), were selected as candidates for metallurgical sectioning. The signatures of interest for these three bearings are shown in Figures 20 and 21; note that three signatures of interest were selected on the piece 470V(2). Specimen 470V(2) was selected for metallurgical sectioning at all three signature locations. The metallurgical sectioning procedure and results obtained are summarized in the section which follows.

D. Metallurgical Sectioning

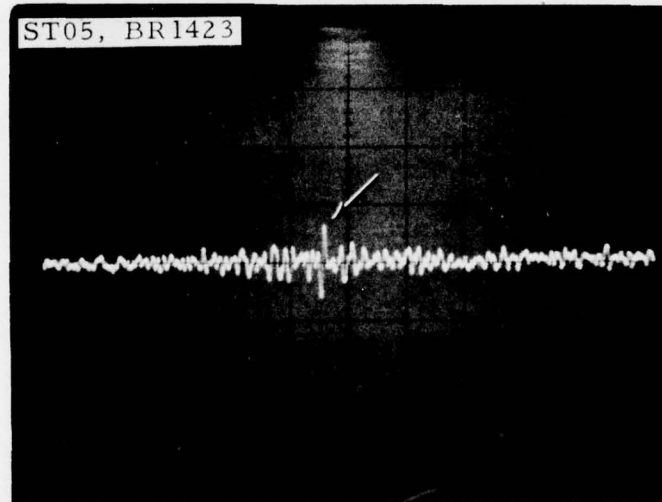
Preparation for sectioning of inner bearing race half 470V(2) at the three signal locations was conducted using the following procedure. The circumferential signature location was accurately established using expanded sweep (horizontally expanded) signature records. Using a sharp scribe, lines were placed on either side of the signal location (with a separation of approximately 0.070 inches (0.175 cm) measured circumferentially about the signature location (see lower photograph in Figure 23). These scribe lines were used as "magnetic markers" as illustrated in Figure 22. Here the signatures from the three corresponding signatures of interest, previously shown in Figure 21, can be seen, respectively, near the center of each of the three records with signatures from the scribe line (SL) on either side. From the magnetic traces shown in Figure 22, the location of the flaw was accurately calculated assuming that the zero crossing of the signal corresponded to the centroids of the defects and the scribe lines. Experience has established that the accuracy of this procedure permits specification of defect locations within ± 0.005 inch (0.125 mm). Figure 23 illustrates the method using a radial signature from a surface flaw.

The upper record, Figure 23, shows the radial signature obtained prior to addition of the scribe lines; the center record shows signatures from the flaw and the scribe lines placed on either side; the lower surface photomicrograph shows both the scribe lines and the

3984



Bearing Inner Race S/N 2079(0)

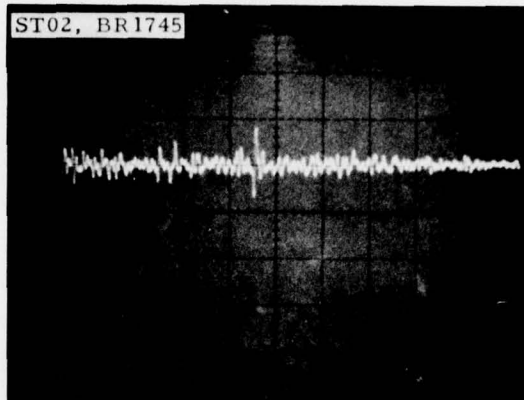


Bearing Inner Race S/N 2298(0)

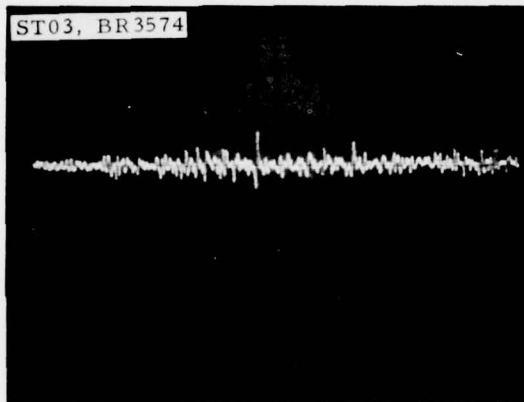
Vertical Sensitivity 0.5 V/div
Horizontal Sweep 1 msec/div
Circumferential Flux, High Field

FIGURE 20. CIRCUMFERENTIAL MAGNETIC PERTURBATION SIGNATURES FROM SELECTED P/N 1-300-015 INNER RACES

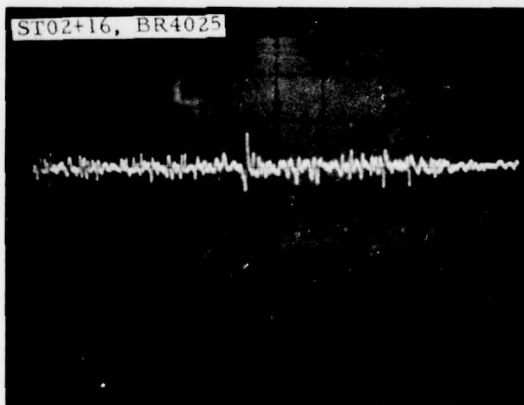
3982



Location A Signature



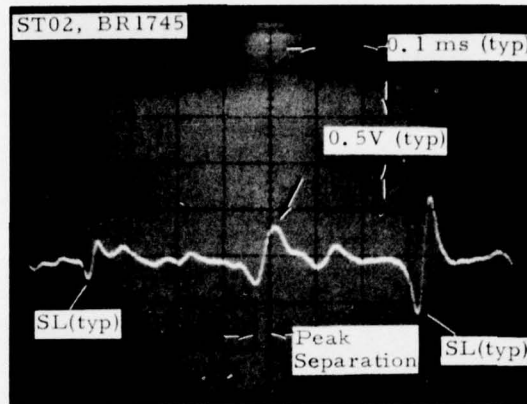
Location B Signature



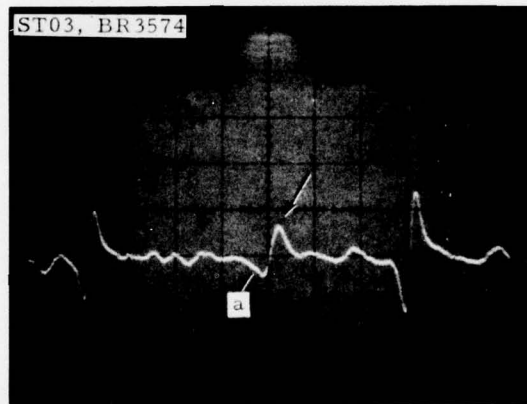
Location C Signature

Vertical Sensitivity 0.5 V/div
Horizontal Sweep 1 msec/div

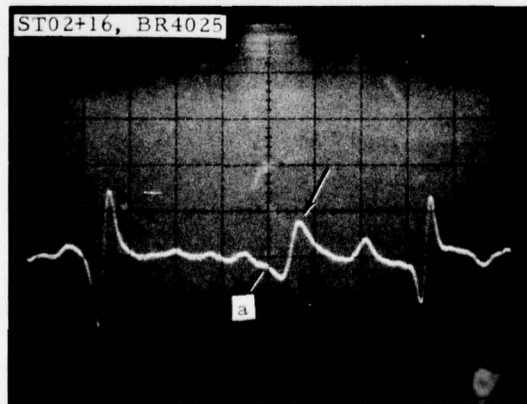
FIGURE 21. CIRCUMFERENTIAL MAGNETIC PERTURBATION SIGNATURES FROM THREE LOCATIONS ON P/N 1-300-015, S/N 470V(2) INNER RACE (HALF)



Location A Signature



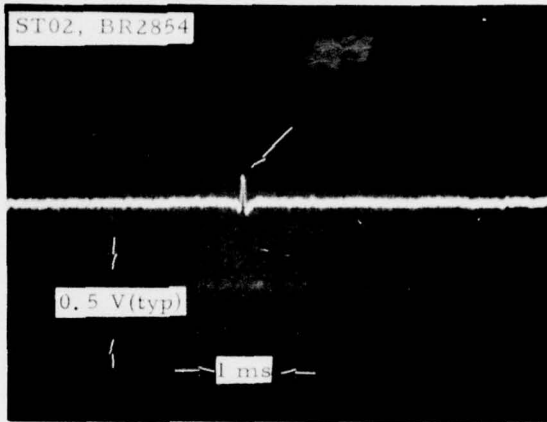
Location B Signature



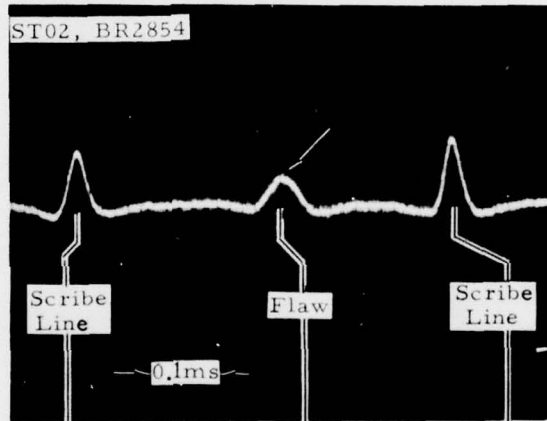
Location C Signature

FIGURE 22. CIRCUMFERENTIAL SIGNATURES (with scribe line signals expanded) FROM THREE LOCATIONS ON P/N 1-300-015, S/N 470V(2) INNER RACE (HALF)

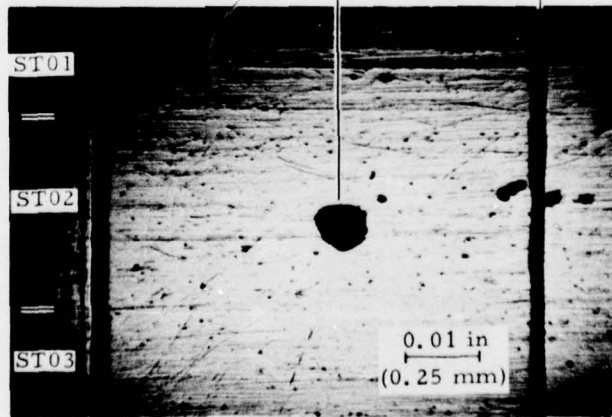
3983



Surface Flaw Signature (before scribe lines)



Surface Flaw and Scribe Line Signatures



Surface Photomicrograph

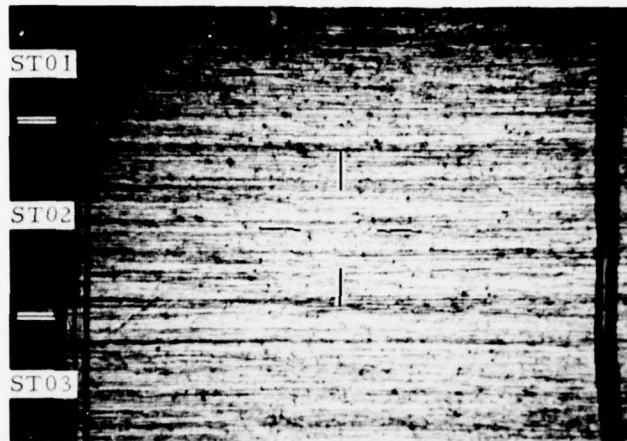
FIGURE 23. MAGNETIC PERTURBATION RADIAL SIGNATURES AND SURFACE PHOTOMICROGRAPH ILLUSTRATING METHOD FOR ACCURATELY DETERMINING FLAW SIGNATURE LOCATION ON RACE (P/N 1-300-015, S/N 455Z(2))

flaw. In the case of these radial signatures, the location of the flaw with respect to the scribe lines was calculated assuming the peak of each of the radial signals corresponded to the centroid of the defect and that of each scribe line. The procedural test illustrated in Figure 23 resulted in a flaw location prediction within approximately 0.001 inch (0.025 mm) of the location physically measured on the surface of the specimen.

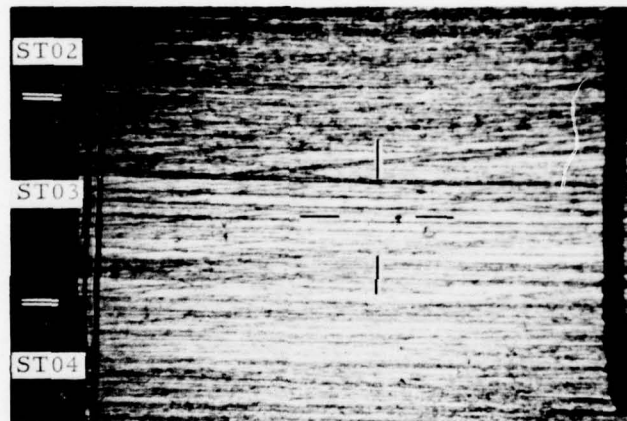
After establishing the apparent defect location, a sector of the race 470V(2) was removed and the cut surfaces made parallel by grinding; then the flaw location was determined by referencing from a ground face to the scribe lines. Subsequently, material was removed from one ground face to provide a "start" sectioning plane within approximately 0.005 inch (0.125 mm) of the predicted location. The three selected signature location specimens were then cast in a single mount for metallographic polishing, and consecutive layers 0.00025 to 0.0005 inch (0.006 to 0.012 mm) were carefully removed. Between each removal, the predicted transverse location of the defect region was scanned via optical microscopy ($\sim 100X$). When a defect was located, metallographic examination was conducted with magnifications up to 750X for the specimen in both the etched (5% nital) and unetched conditions.

Figure 24 shows surface photographs of the raceway surface of the three regions corresponding to the signatures previously presented in Figures 21 and 22. The reticle in each of the photographs of Figure 24 indicates the projected flaw locations; no significant surface indications are present. A small subsurface inclusion, approximately 0.0006 inch (0.015 mm) in diameter and approximately 0.002 inches (0.050 mm) beneath the surface was found to correlate with the signature at Location A (see Figures 21 and 22) as illustrated in Figure 25. No significant flaws were found corresponding with locations B and C (reference Figures 21 and 22). It is informative to re-examine the signatures at locations A, B and C in Figure 22 in terms of the details of signature characteristics. The location A signature had good symmetry and shape with a peak separation of approximately 0.0036 inch (0.09 mm) and extended over about one scan track width 0.02 inches (0.50 mm). Location B and C signatures extended at least two scan track widths across the ball groove and the records in Figure 22 show both signatures to have poor symmetry (downward-going peak less in amplitude than upward-going peak); peak separations in the range of 0.0025 to 0.003 inch (0.063 to 0.075 mm). Also note that the location B and C signatures have a poor shape leading into the downward-going as indicated by the "a" in the records of Figure 22. Signatures such as B and C, if from an inclusion, would be anticipated to be associated only with a group ("cloud") of small [less than 0.0005 inch (0.012 mm) diameter], subsurface inclusions distributed across the ball groove. However, no such flaws

3985



Location A (ST02, BR1745)



Location B (ST03, BR3574)



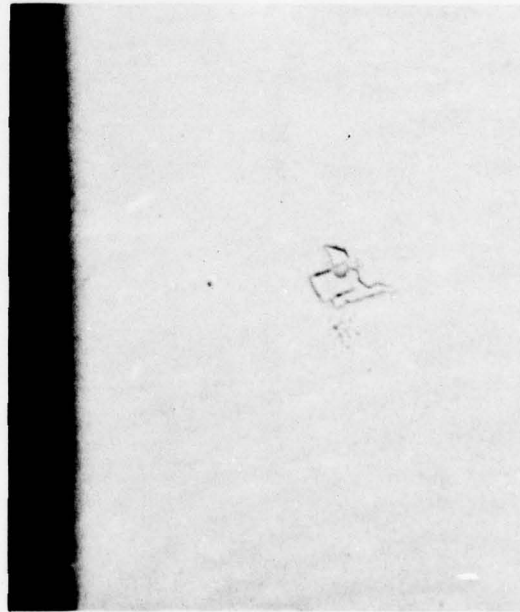
Location C (ST02+16, BR4025)

FIGURE 24. SURFACE PHOTOMICROGRAPHS OF REGIONS (Locations A, B, C) CORRESPONDING TO THREE SIGNATURES ON P/N 1-300-015, S/N 470V(2) INNER RACE (HALF)

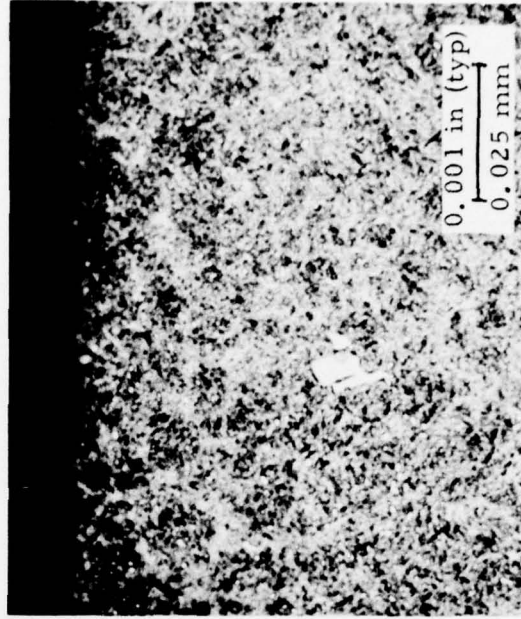
3980



Location A Signature



Unetched



Etched

FIGURE 25. MAGNETIC PERTURBATION CIRCUMFERENTIAL SIGNATURE AND CORRESPONDING SUBSURFACE FLAW, P/N 1-300-015, S/N 470V(2) INNER RACE (HALF)

were found in the region examined. Accordingly, it is suggested that the signatures B and C were caused by slight local metallurgical composition changes such as fiber flow; the signature extent (1.0 mm) across the race groove and the small amplitude are the primary factors supporting this suggestion. Also, while an inclusion was found to coincide with signature A, the inclusion approaches the lower limit which could possibly be resolved at this depth from the magnetic background signatures.

IV. OTHER RELATED RESULTS

The detection of near subsurface nonmetallic inclusions and the influence of such flaws on bearing service life is emphasized by recent results obtained from endurance testing main shaft bearings from the No. 4 position in the J57 engine for the Air Force (Contract No. 09603-74-C-5158). Magnetic perturbation, Barkhausen noise, and laser scattered light inspections were conducted on reparable reject J57-#4 bearings; two bearings selected from the group were placed on endurance test based on the inspection results. The endurance tests were conducted at 8700 rpm under a 15,000 pound load providing a calculated maximum initial Hertz stress of 332,000 psi on the inner race of the bearing (assuming a contact angle of 24.5° and a race curvature of 52%). Automatic shutdown of the endurance test rig occurred after 16 hours of test time and an investigation showed that shutdown was actuated by the vibration monitor; disassembly revealed that the loaded half of the inner race (S/N S10161) contained a spall approximately 0.4-inch (1 cm) in diameter.

From subsequent comprehensive correlation analyses, it was determined that the spall initiated from a source corresponding to the precise location of an outstanding magnetic perturbation circumferential signal obtained prior to start of the endurance test. Furthermore, the specific signature was the basis for selecting the bearing for endurance testing from a large group screened to obtain candidate specimens. Figure 26 is a reproduction of the initial inspection printout. Note that no magnetic perturbation radial or laser light signals corresponding to the magnetic perturbation circumferential signal at BR 4850 was obtained; also there was no significant surface flaw present in this region prior to endurance testing. Figure 27 shows a surface photomicrograph of the leading edge of the spall as a result of testing and a reproduction of the circumferential inspection record obtained prior to testing in the region of the BR 4850 printout; note the outstanding signal present in the inspection record. The peak separation of the signature, obtained prior to endurance testing, was 0.0025-inch (0.063 mm) indicating the presence of an inclusion whose center was approximately 0.001-0.002 inch (0.025-0.050 mm) beneath the raceway surface. In the photomicrograph of the leading edge of the spall, the site of the inclusion corresponding to the BR 4850 location is pointed out by the arrow (the small arrows point out a crack). These endurance test results clearly establish the critical role that such small nonmetallic flaws can play in the service life of expensive and critical bearing components. Furthermore, the initiation of failure at the precise location predicted by the magnetic perturbation signature prior to endurance testing establishes the capability of these inspection methods to detect critical flaws in bearings - -

Bearing Serial No., J57-#4, Inner Race, Loaded Half
ENTER BEARING PARAMETERS SEPARATED BY A COMMA OR SPACE
11 S10161@6599 056 0 2 0 1 0 M B L
ENTER THE FOLLOWING 21 DIGITS ON THE TAPE ENCODER
1 1 8 3 6 4 1 0 1 6 1 6 5 9 9 0 5 6 2 2 0
TYPE YES WHEN DONE YE

LOAD P-TAPE NO. 110
TYPE YES WHEN DONE YE
LOAD BEARING, CLOSE DOOR, THEN TYPE YES YE

ENCODER READING AT BEARING REF. MARK DETECTION 2967
BEARING REF. MARK FROM SHAFT ZERO 4725

FLAWS
TY S T B R S R
CH 0007 4850 4575

Legend: CH-Circumferential Flux High
Flux Density
ST-Probe Position Across Race
BR-Circumferential Position From
Ref. Scribe Line

Note: Bearing was selected for endurance
testing on basis of signal @ 0007 and 4850

DECREASE TAPE SPEED TO 3.75 IPS, THEN TYPE YES YE
INCREASE TAPE SPEED TO 30.0 IPS, THEN TYPE YES YE

ENCODER READING AT BEARING REF. MARK DETECTION 2967
BEARING REF. MARK FROM SHAFT ZERO 4725

ENCODER READING AT BEARING REF. MARK DETECTION 2967
BEARING REF. MARK FROM SHAFT ZERO 4725

FLAWS
TY S T B R S R
LA 0000 3182 2907
LA 0001 3182 2907
LA 0002 3157 2882
LA 0002 3205 2930
LA 0003 3170 2895
LA 0004 3170 2895
LA 0010 2633 2358
LA 0012 1028 0753
LA 0012 4161 3886

DO YOU WANT VISUAL INSPECTION? (YES OR NO) NO
DO YOU WANT A MANUAL INSPECTION? (YES OR NO) YE
MANUAL MODE. RESPONSE TO PROCEDURE? SHOULD BE MP FOR
MAG. PERT. BK FOR BARKHAUSEN, LS FOR LASER, EN FOR END
PROCEDURE? MP
RESPOND TO ? BY TYPING
HF FOR HIGH FIELD, LF FOR LOW
STXX TO GO TO SCAN TRACK XX
APXX TO ADVANCE PROBE XX STEPS
DPXX TO DECREMENT PROBE XX STEPS
RN TO END PROCEDURE AND RETURN
? HF
? ST07
? RN
PROCEDURE? EN
DO YOU WANT TO RERUN? (YES OR NO) NO
UNLOAD THE BEARING, THEN TYPE YES YE

FIGURE 26. PRINTOUT OBTAINED FROM INSPECTION OF J57-#4
BEARING PRIOR TO ENDURANCE TEST

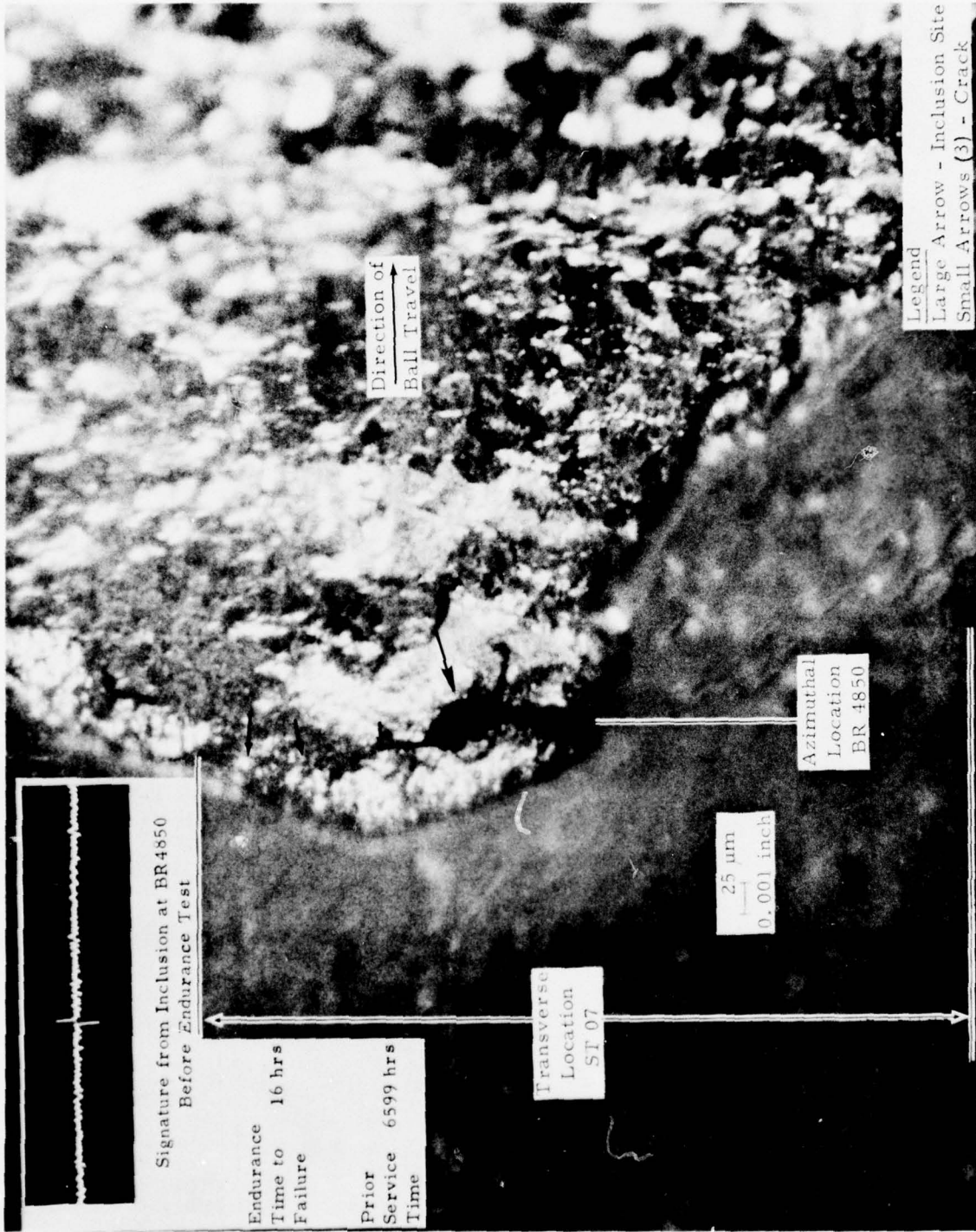


FIGURE 27. PHOTOGRAPH OF LEADING EDGE OF SPALL AND INSPECTION SIGNATURE OBTAINED PRIOR TO ENDURANCE TESTING

no other nondestructive inspection method currently known has such a capability. It is emphasized that this race was manufactured from CEVM/VAR material. From the fact that the bearing failed at the inclusion in the load track after only 16 hours endurance time, it is suggested that the prior 6599 hours actual service time in J57 engines had already caused subsurface cracks to develop at the inclusion and the bearing was "primed" for failure. Furthermore, it is reasonable to suggest that the bearing would have been returned to service after rework and that the subsurface flaw would have caused the bearing to fail in service if it had not been detected in the CIBLE equipment.

V. CONCLUSIONS AND RECOMMENDATIONS

As a result of the design, fabrication, verification testing and analyses of the bearing diagnostic test system which utilizes magnetic perturbation and Barkhausen noise methods, it is clearly evident that the system facilitates a rapid, definitive and critical nondestructive inspection of the active regions of bearing raceways. Comparison of inspection results from the preliminary prototype unit and the prototype system verifies a system-to-system reproducibility; amplitude within $\pm 15\%$; detailed signal characteristics and magnetic background repeatability are excellent; signal location within ± 0.005 inch (± 0.125 mm). Capability of the magnetic perturbation method to detect sub-surface flaws was demonstrated via metallurgical sectioning. Stress assessment capability of the Barkhausen noise method was clearly demonstrated by the application of bending stresses to a bearing race in the laboratory.

As a continuation of the CIBLE program, it is recommended that additional efforts be undertaken to provide a comprehensive data base on Army bearing components for establishing a serviceability criteria based on measured condition of individual components. The following elements should be included:

- 1) Inspect a significant number of new bearings and after accumulation of service time in engines, re-inspect these bearings at engine overhaul; re-inspect again after a second service tour.
- 2) Inspect bearings to be refurbished and or reworked prior to and subsequent to processing; re-inspect the refurbished reworked bearings after one engine overhaul period.
- 3) Inspect a significant number of reject bearings (rejection based on anomalies and flaws in raceway other than major spalls) and compare findings using current conventional inspection methods with those obtained from the bearing diagnostic test equipment.
- 4) Inspect new, service, refurbished, reworked and/or reject bearings. Select bearings for laboratory endurance test to augment performance data from bearings in a "service" environment.

- 5) Select bearings from steps 1), 2), 3), and/or 4) for metallurgical investigation to aid in developing quantitative correspondence between bearing conditions and signature characteristics.
- 6) Develop an automatic signature characterization, data compression and analysis system for use with the bearing diagnostic test equipment to facilitate the analysis of signatures, the storage and retrieval of selected signatures, and "accept"- "reject" decisions based on a continuously updated serviceability criteria.

Furthermore, it is suggested that the above efforts should be closely coordinated with similar efforts being conducted on Air Force bearing components by Southwest Research Institute. It is recommended that inspection data and results from both the Army and Air Force programs be resident in the same overall data base management system - such an arrangement would be mutually beneficial and cost effective.

VI. REFERENCES

1. Bohm, K. , Schlicht, H. , Zwirlein, O. , and Eberhard, R. , "Nonmetallic inclusions and Rolling Contact Fatigue," Bearing Steels: The Rating of Nonmetallic Inclusions, ASTM STP 575, American Society for Testing and Materials, 1975, pp. 96-113.
2. Kusenberger, Felix N. , Bradshaw, William W. , and Barton, John R. , "Inspection of Refurbished Helicopter Engine and Transmission Bearings Using Magnetic Perturbation, Barkhausen Noise and Laser Light Methods," SwRI Project No. 15-4018, Under Army Contract No. DAAG46-74-C-0143 dated January 1975.

APPENDIX

**BEARING INSPECTION EQUIPMENT
DEVELOPMENT HIGHLIGHTS**

Magnetic Perturbation Development

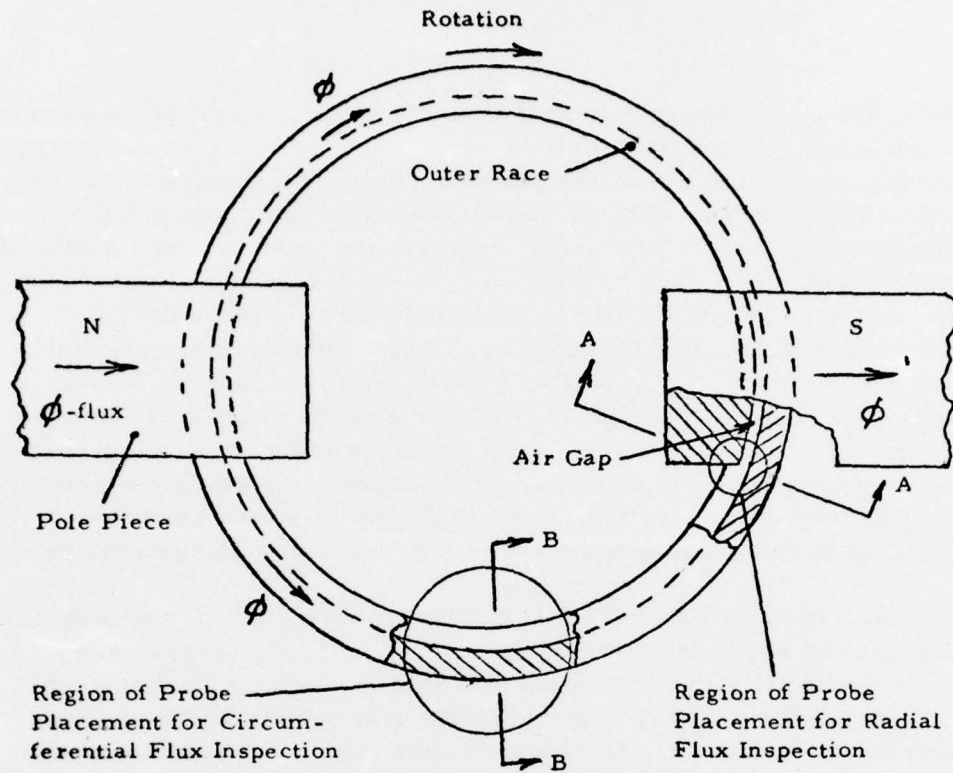
Both Hall effect and wire coil type magnetic perturbation sensors were investigated. Many parameters were considered, viz., uniformity of sensitivity over the width of the sensor (dimension across the raceway), repeatability of inspection, associated electronic circuitry requirements, fabrication problems, probability of achieving a practical probe design, and impact on overall equipment design. The wire coil type of sensor was selected for the equipment development based on its uniform sensitivity, simplicity of design, relatively simple external circuit requirements, its compatibility with high scan speed (faster inspection), and SwRI's in-depth experience and the repeatable fabrication of essentially identical units based on experience from other magnetic perturbation systems. The wire coil type sensor was also selected for the Barkhausen noise method since this type of sensor has been used solely in Barkhausen noise laboratory and developmental systems to date.

Several wire coil probe configurations were considered from the standpoints of suspension and coupling. Two basic approaches evolved, i) multiple wire coils encapsulated in a single package, the number of wire coils sufficient to cover the transverse width of the active bearing raceway and ii) a single wire coil encapsulated in a package which could be sequentially indexed to adjacent tracks across the bearing raceway. The latter or single coil package approach was selected for its simplicity of design and fabrication, its ability to accommodate tolerance in ball groove curvature, its capability to achieve as much track overlap as desired, and its relative economy of fabrication.

The overall design objective was a system for inspecting both inner and outer bearing races using a common rotational and magnetizing unit with a minimum requirement for independent fixturing to accommodate each different type of bearing element. The magnetizing pole piece configuration selected is illustrated in Figure A1 (for an outer race); the outer race is selected for illustration here since it is the most difficult configuration for the installation and removal of pole pieces and sensors as part of the inspection procedure. Figure A1 shows schematically the placement of the two different types of magnetic perturbation probes, i. e., the radial and circumferential. Accommodation of the Barkhausen sensor was achieved later by placing it in a position similar to that used for the circumferential magnetic perturbation probe.

Figures A2 and A3 show views of the preliminary prototype inspection head during development. Several of the more significant

3005



Note: Loading and unloading of the ring is accomplished by moving pole pieces toward each other to clear raceway, lowering ring below pole pieces, then moving pole pieces apart to clear O. D. of the ring.

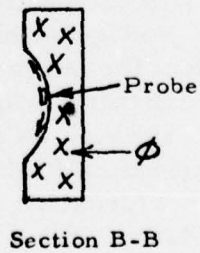
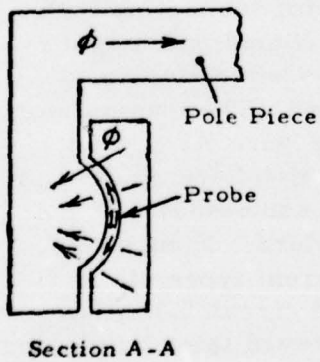


FIGURE A1. MAGNETIZATION AND PROBE CONFIGURATION FOR OUTER RING

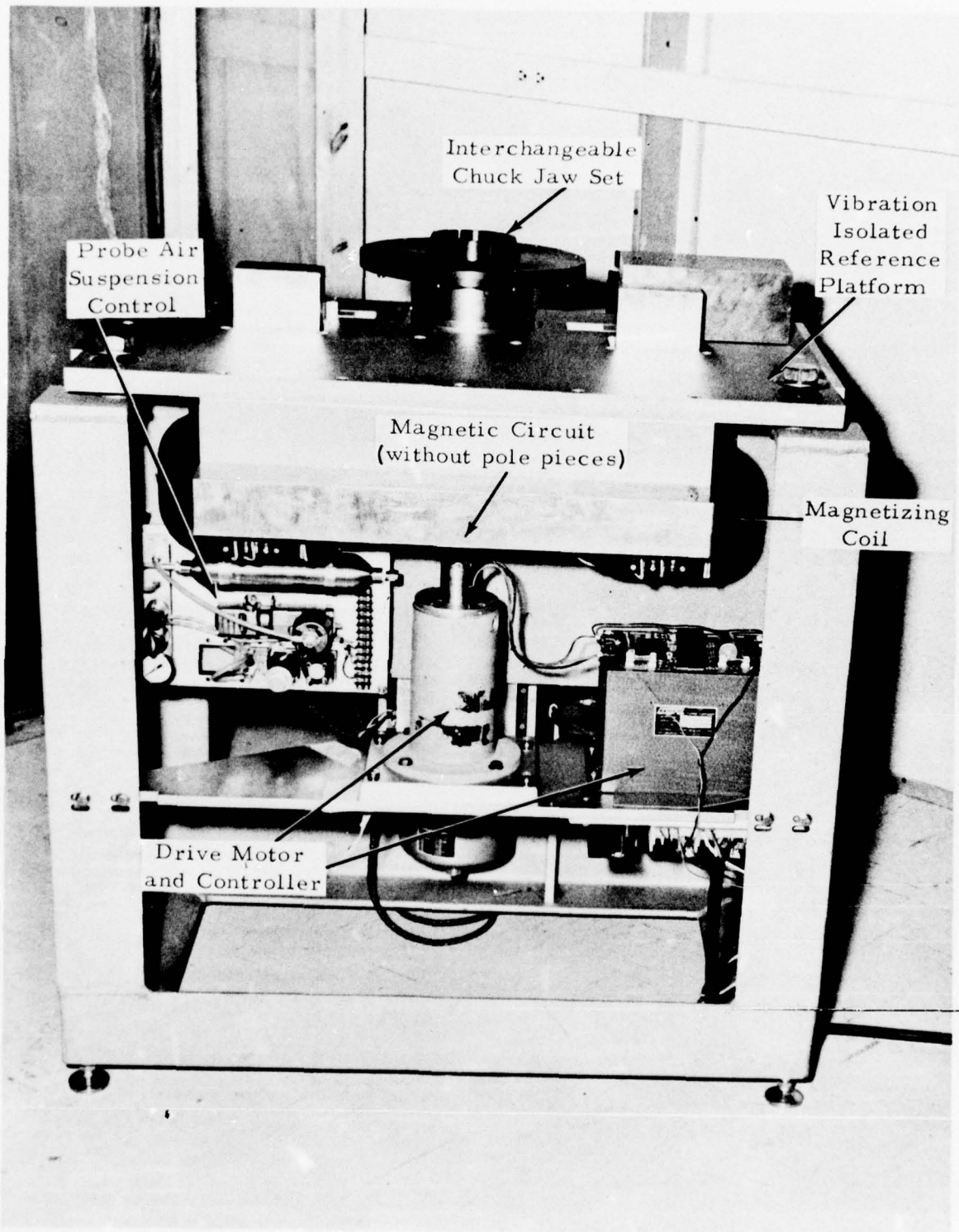


FIGURE A2. REAR VIEW OF BEARING INSPECTION DEVICE ROTATING AND MAGNETIZING SUBASSEMBLY (Preliminary Prototype)

3053

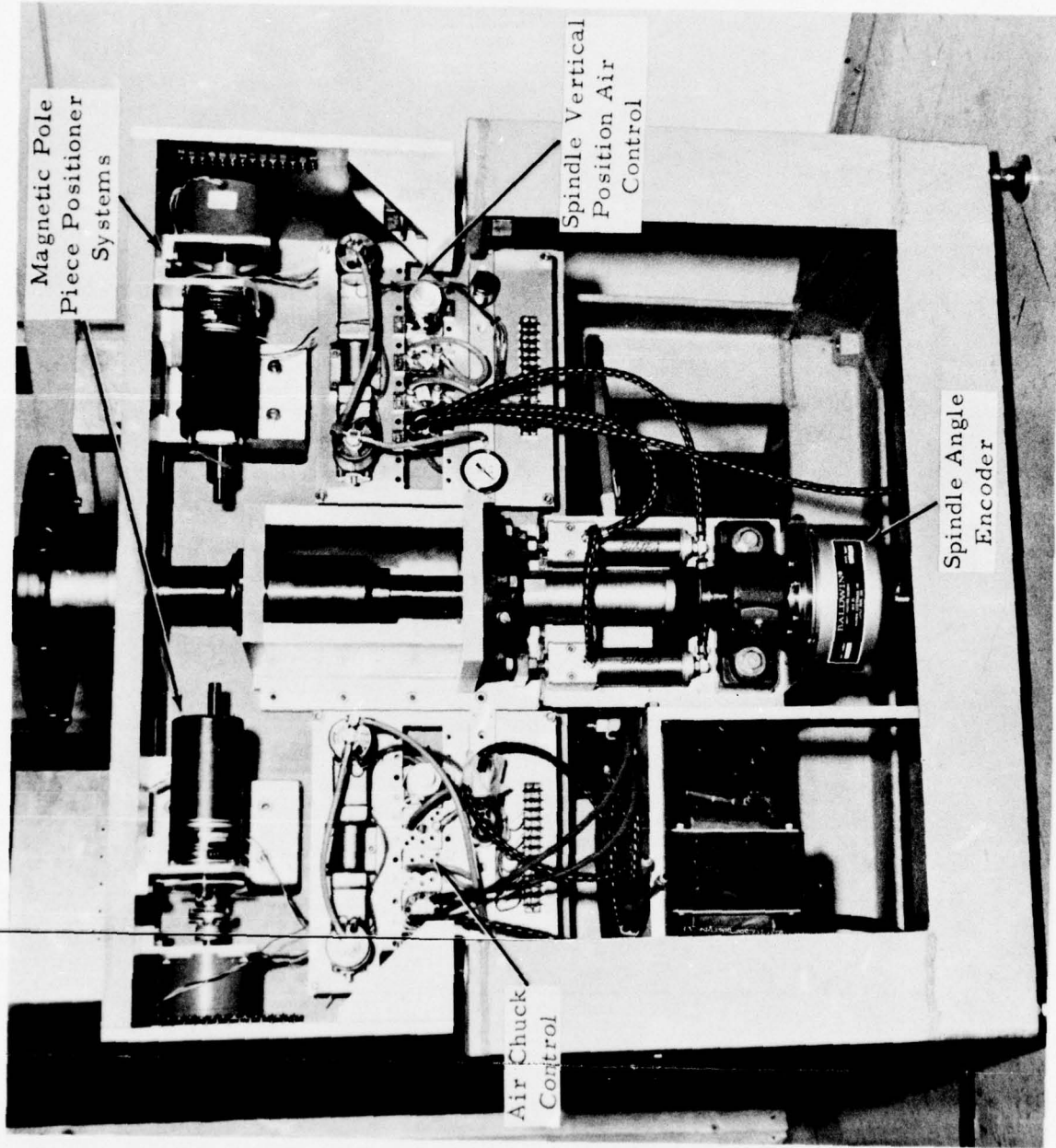


FIGURE A3. FRONT VIEW OF BEARING INSPECTION DEVICE ROTATING AND MAGNETIZING ASSEMBLY (Preliminary Prototype)

items in the assembly are pointed out in these figures. In the delivered prototype (CCAD) system, a commercial spindle was used for rotation of the bearing; however, because of a 26-week delivery quotation, a spindle was designed and fabricated for the preliminary prototype. The design of the fabricated spindle was made similar to the commercial item such that it is possible to directly replace it with a commercial unit.

Figure A4 shows an overall view of the preliminary prototype inspection head with a pair of pole pieces mounted (the computer, computer interfacing and teleprinter shown are equipment furnished by SwRI during the development). Figure A5 shows a closeup view of probe mechanisms mounted on each pole piece position within an outer race for inspection. The probe mechanism configuration shown in Figure A5 is an early developmental version in which the radial probe mechanism was mounted on one pole piece and the circumferential probe mechanism mounted on the other pole piece. A single package circumferential/radial probe configuration was developed such that one basic platform attached to one of the two pole pieces for the radial and circumferential magnetic perturbation inspection; a second mechanism for the Barkhausen inspection was attached to the other pole piece. Figure A6 shows a view of a typical set of parts for a magnetic perturbation circumferential/radial probe mechanism; a typical Barkhausen probe mechanism is similar with the exception that no probe or probe suspension mechanism is attached in the radial probe location - - the Barkhausen probe mounts in the circumferential probe location of the mechanism.

Barkhausen Noise Development

Barkhausen noise state-of-stress measurements on antifriction bearing races are based upon a broad background of Barkhausen noise measurements on steel conducted by SwRI over the past 10 years, and more directly on Barkhausen noise stress measurements conducted on bearing races before and after service under Air Force Contract No. F09603-70-D-5547 by SwRI in 1973-1974. The significance of the results of the Air Force program is illustrated by Figure 2 in the Introduction to this report. The results reported in Figure 2 were obtained by what will be referred to here as the "conventional" Barkhausen approach and is one in which i) a slowly time-varying magnetic field is applied to the part being inspected, ii) the probe fixed in position on the specimen, and iii) the resulting Barkhausen noise processed electronically to produce the typical signatures illustrated in this figure. This conventional approach, however, permits stress measurement only by sampling specific regions; accordingly, the time

3137

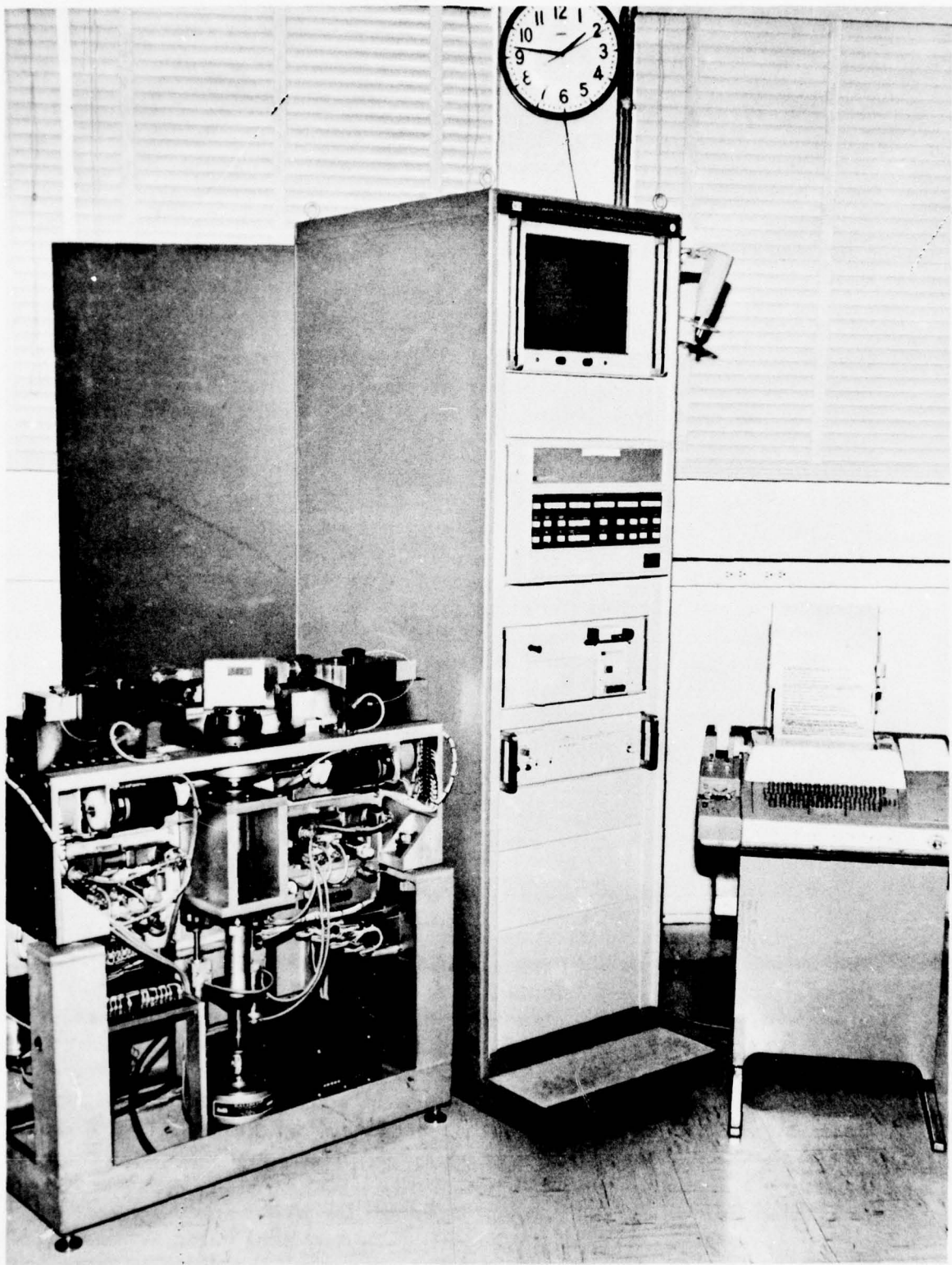


FIGURE A4. OVERALL VIEW OF PRELIMINARY PROTOTYPE BEARING INSPECTION UNIT

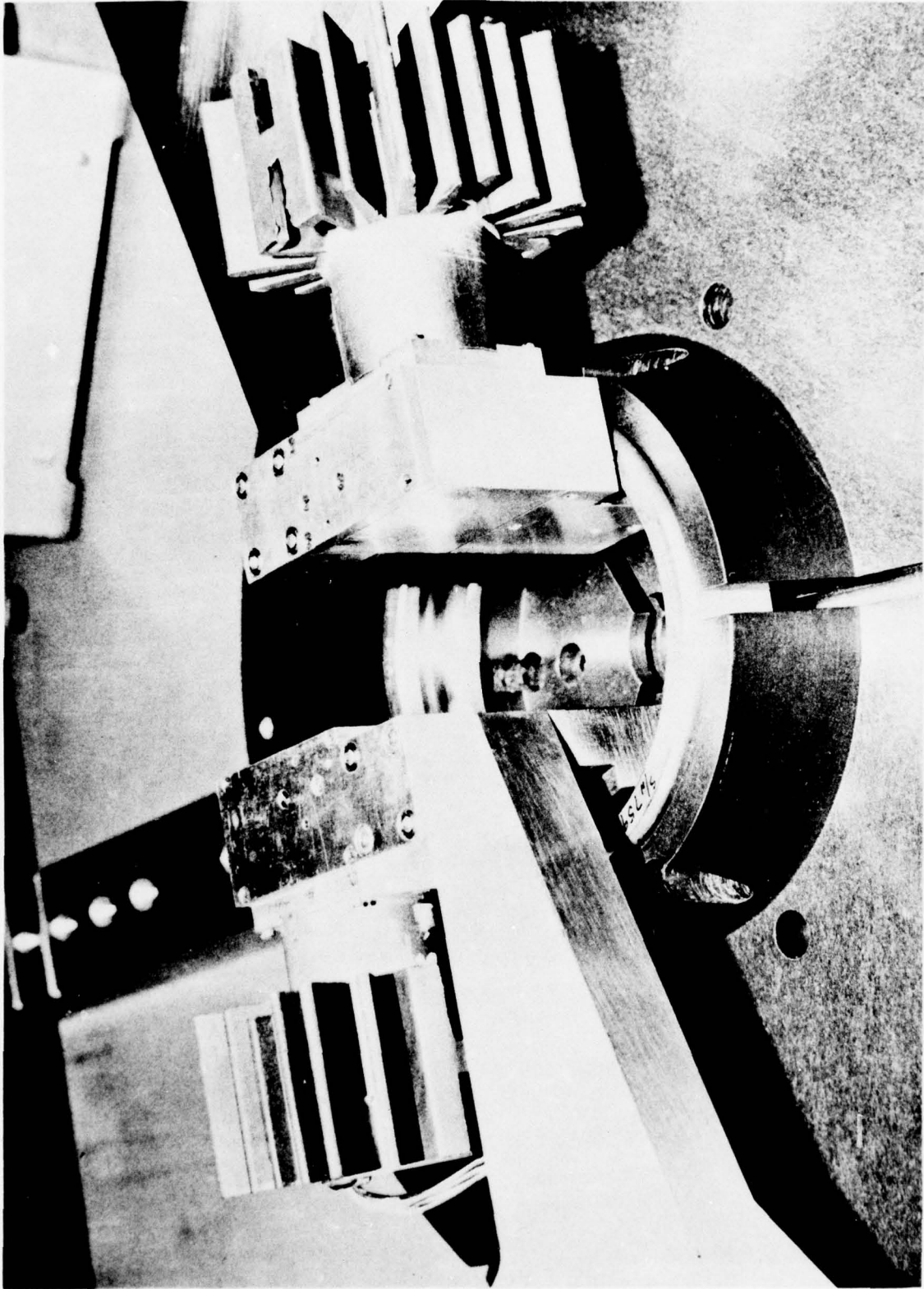


FIGURE A5. CLOSE-UP VIEW OF PROBE MECHANISMS WITHIN OUTER RACE (in position for inspection)

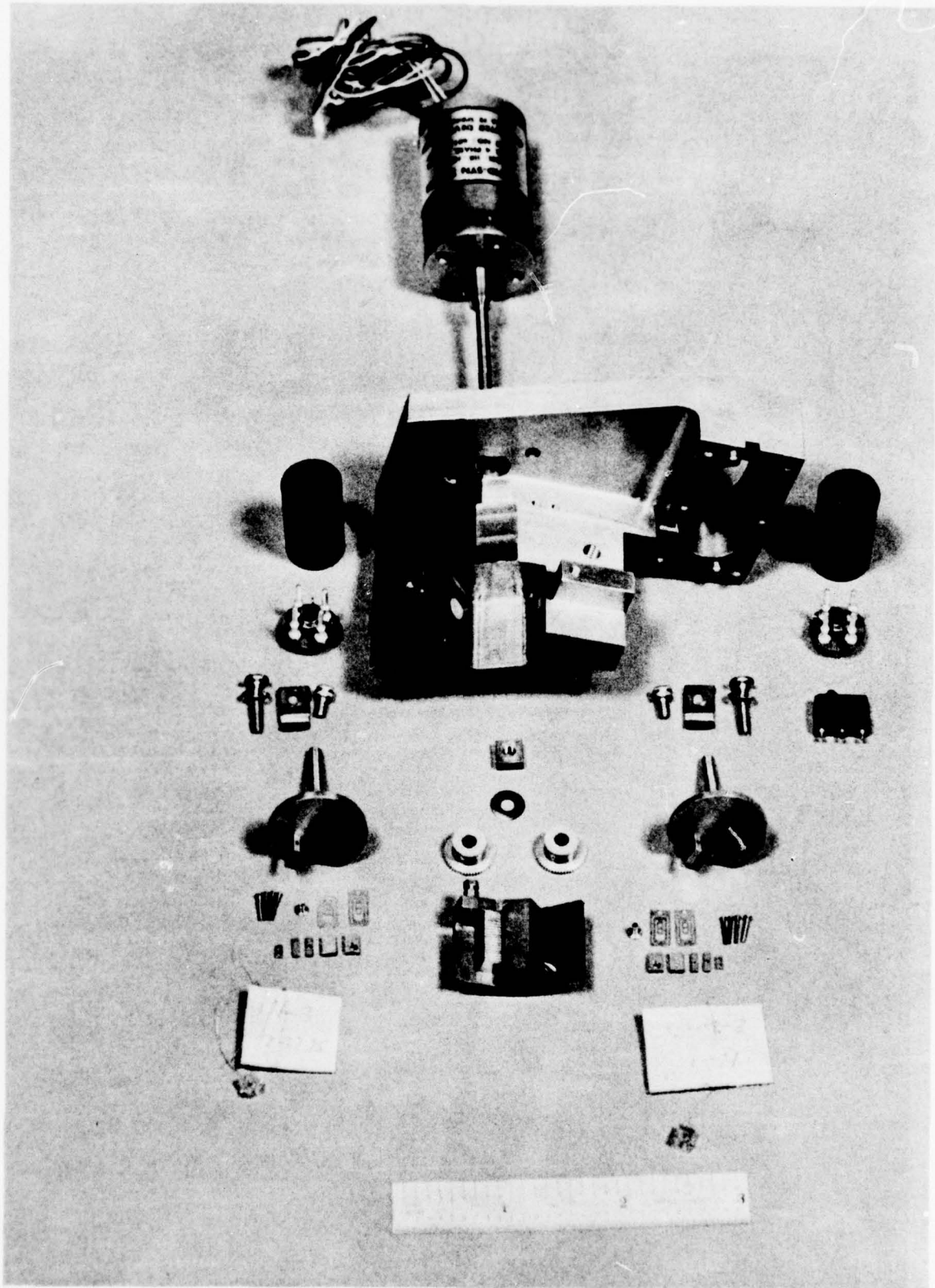


FIGURE A6. VIEW OF TYPICAL SET OF PARTS FOR A MAGNETIC PERTURBATION CIRCUMFERENTIAL RADIAL PROBE MECHANISM

required to examine a fine matrix of adjacent regions over any significant surface area is perhaps prohibitive for routine inspection. For this reason, before undertaking the finalized implementation of the conventional Barkhausen approach for bearing inspection, an alternate approach referred to hereafter as the "continuous" Barkhausen approach, conceived several years ago by SwRI, was investigated from the implementation point of view. The continuous Barkhausen approach, conceptually, is one in which the bearing or specimen is moved with respect to the magnetizing circuit and probe and a DC magnetic field is applied - - thus providing a continuous scan capability over the specimen surface.

Initial continuous Barkhausen experimental work was conducted on a flat, tensile specimen of normalized AISI 4130 steel in which indents and shot-peened regions were introduced. The specimen was stressed under various uniaxial tensile loads during the experiments using the apparatus shown in Figure A7; a closeup view of the magnetizing circuit and probe is shown in Figure A8; and the specimen is illustrated in Figure A9. The upper row of records, a through d in Figure A10, illustrates the continuous Barkhausen results obtained. Note strip-chart recordings a and b show the amplitude of continuous Barkhausen to increase with increasing applied uniaxial tensile stress - - note the reduced Barkhausen amplitude obtained from the shot-peened areas pointed out in a and b. Polaroid records c and d show the unprocessed Barkhausen signal for two different levels of tensile stress. Records e through h in Figure A10 illustrate the results obtained using the conventional Barkhausen approach on the same specimen. Note that with increasing applied tensile stress, the conventional Barkhausen signal amplitude increases, compare record f with e. In addition, records g and h show the Barkhausen signature amplitude to be reduced in the shot-peened regions as compared with the nonshot-peened regions, compare records g and h with e and f, respectively. Interestingly, the conventional Barkhausen signatures from the shot-peened region with tensile stress applied behave similar to that noted for some "service" bearing races (see Figure 2) where "spike" signature formation was noted. (Note spike-like signature formation in records g and h of Figure A10.)

The results obtained from a T53 engine main shaft roller bearing (reject) inner race containing a hardness indentation is shown in Figure A11. Photographs showing the laboratory setup and specimens are presented in Figures A12 and A13. It was found that continuous Barkhausen increased, monotonically, with rotational speed over the range investigated (approximate 1-7 ips surface speed). Records a through d illustrate that as the magnetizing current is increased, the

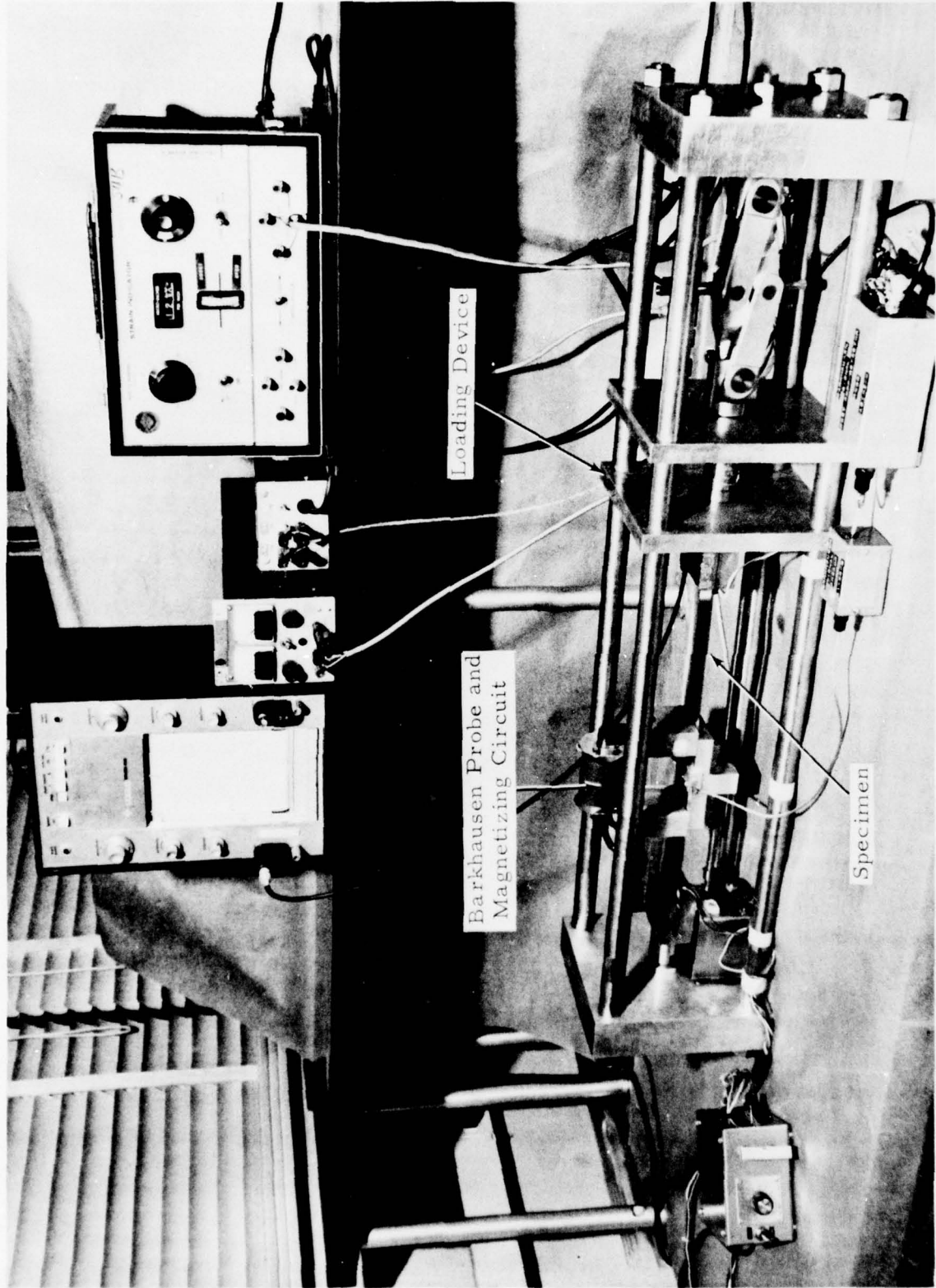


FIGURE A7. CONTINUOUS BARKHAUSEN APPARATUS AND STRESSING FIXTURE FOR FLAT SPECIMEN

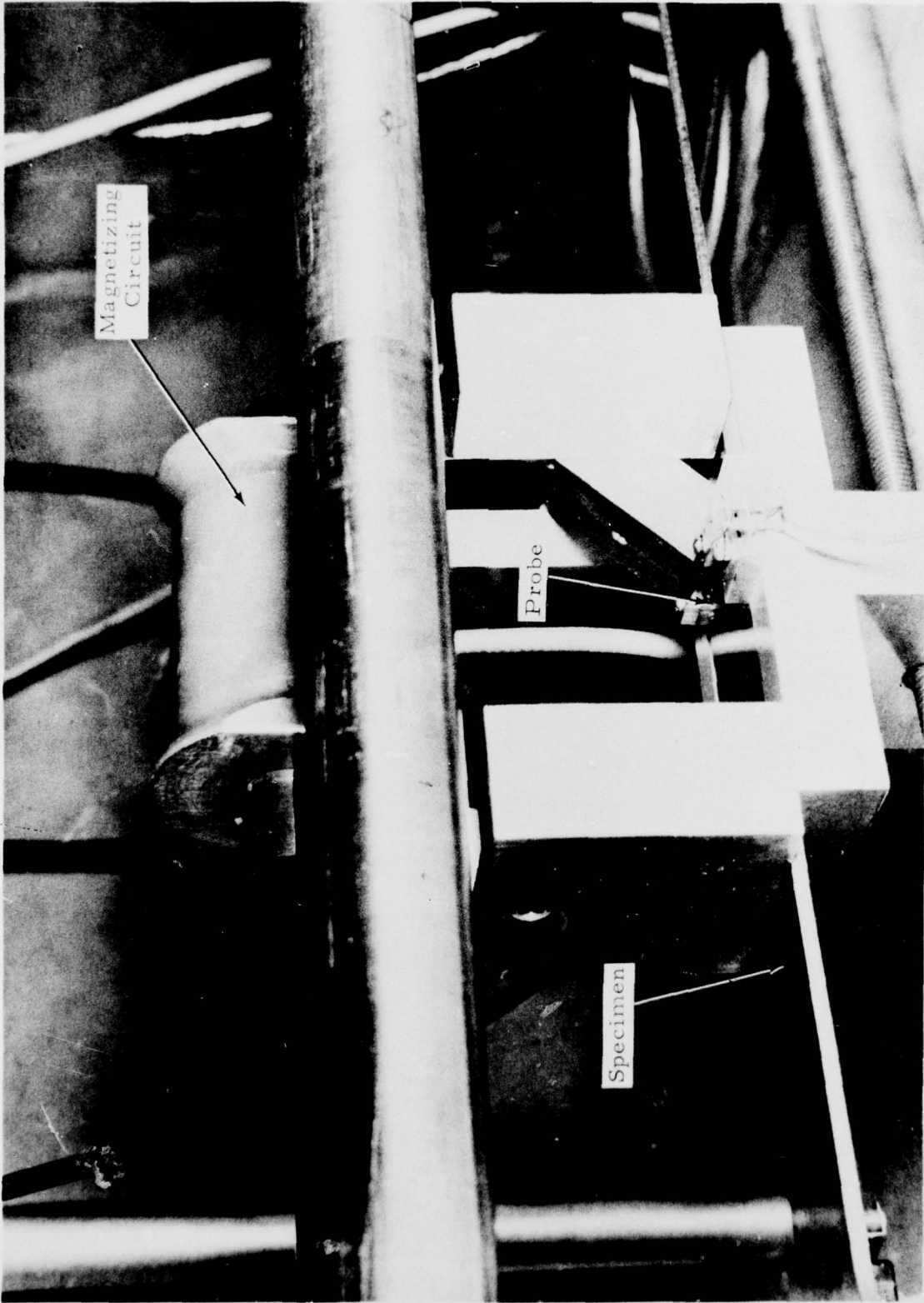


FIGURE A8. CONTINUOUS BARKHAUSEN PROBE, MAGNETIZATION APPARATUS, AND CARRIER ASSEMBLY

4014

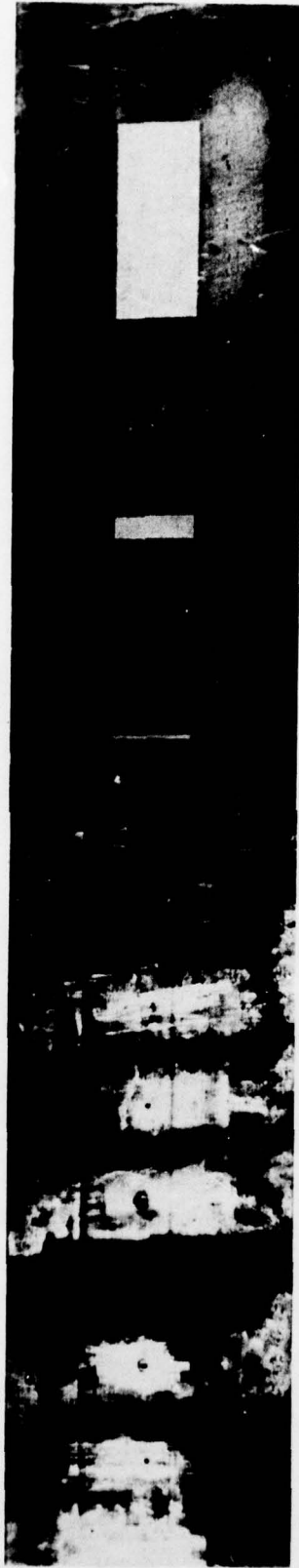
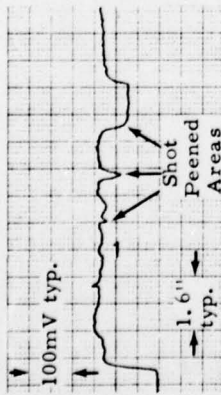
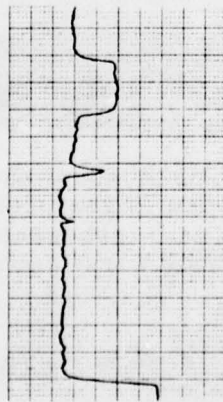


FIGURE A9. 4130 FLAT STEEL SPECIMEN SHOWING SHOT-PEENED AREAS AND INDENTS

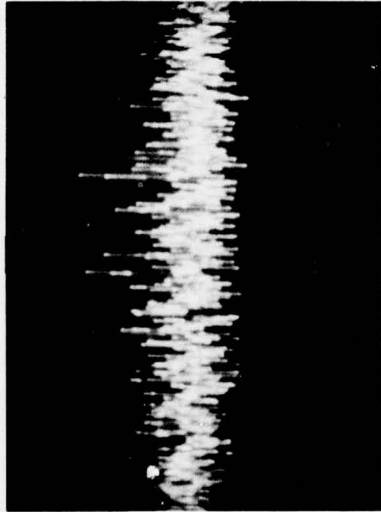
CONTINUOUS BARKHAUSEN



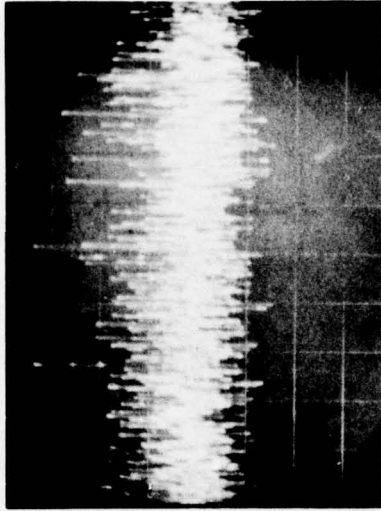
a. Continuous Barkhausen detected signal, 8.5 ksi tension



b. Continuous Barkhausen detected signal, 55 ksi tension

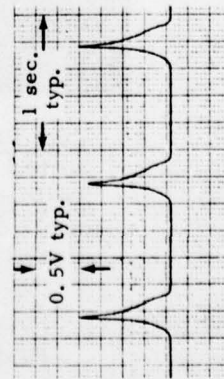


c. Unprocessed continuous Barkhausen signal 10 ksi tension, vert. 0.2 V/cm, horz. 0.1 s/cm

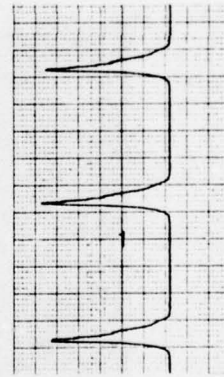


d. Unprocessed continuous Barkhausen signal 45 ksi tension, vert. 0.2 V/cm, horz. 0.1 s/cm

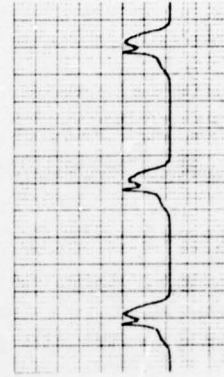
CONVENTIONAL BARKHAUSEN



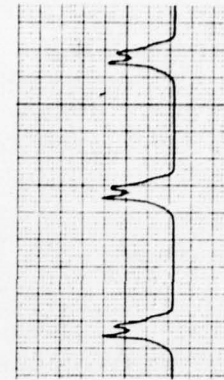
e. Conventional Barkhausen detected signal from unshot-peened area of specimen, 8.5 ksi tension



f. Conventional Barkhausen detected signal from unshot-peened area of specimen, 55 ksi tension

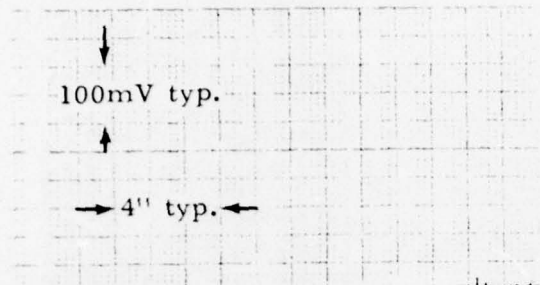


g. Conventional Barkhausen detected signal from shot-peened area of specimen, 8.5 ksi tension

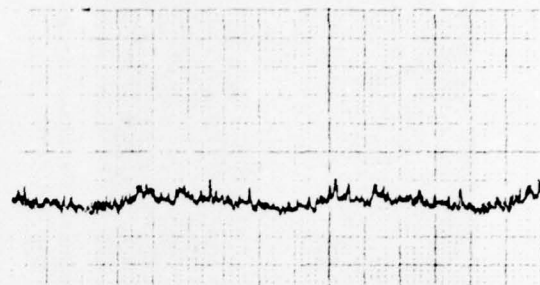


h. Conventional Barkhausen detected signal from shot-peened area of specimen, 55 ksi tension

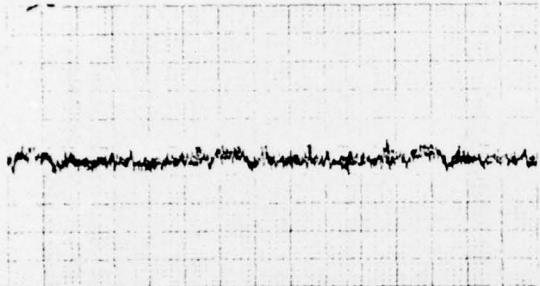
FIGURE A10. CONVENTIONAL AND CONTINUOUS BARKHAUSEN DATA FROM UNSHOT-PEENED AND SHOT-PEENED AREAS ON A FLAT SPECIMEN UNDER DIFFERENT TENSILE LOADS



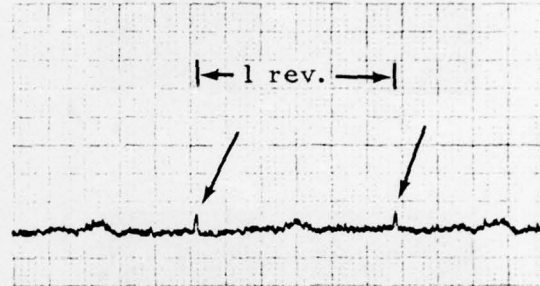
a. Continuous Barkhausen detected signal, 0 Amp magnetizing coil current



b. Continuous Barkhausen detected signal, 1.0 Amp magnetizing coil current

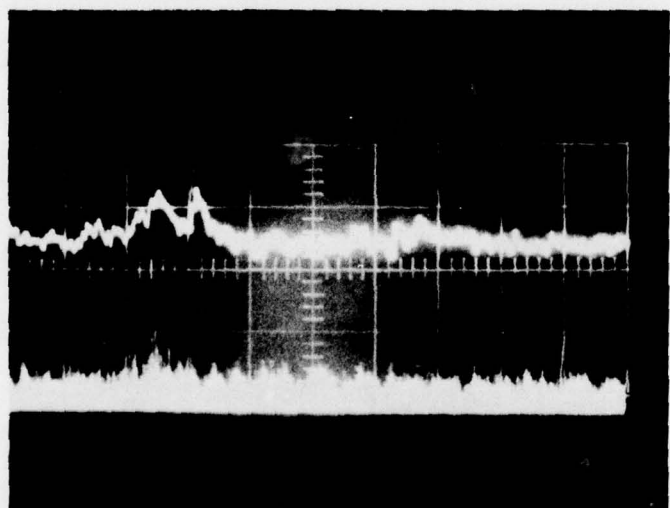


c. Continuous Barkhausen detected signal, 1.5 Amp magnetizing coil current



d. Continuous Barkhausen detected signal, 2.0 Amp magnetizing coil current. Note indent signature.

4015



e. Top Trace: Continuous Barkhausen detected signal showing indent signature.
Bottom Trace: Continuous Barkhausen unprocessed signal showing burst associated with indent.

FIGURE A11. CONTINUOUS BARKHAUSEN DATA FROM A ROLLER BEARING RACE

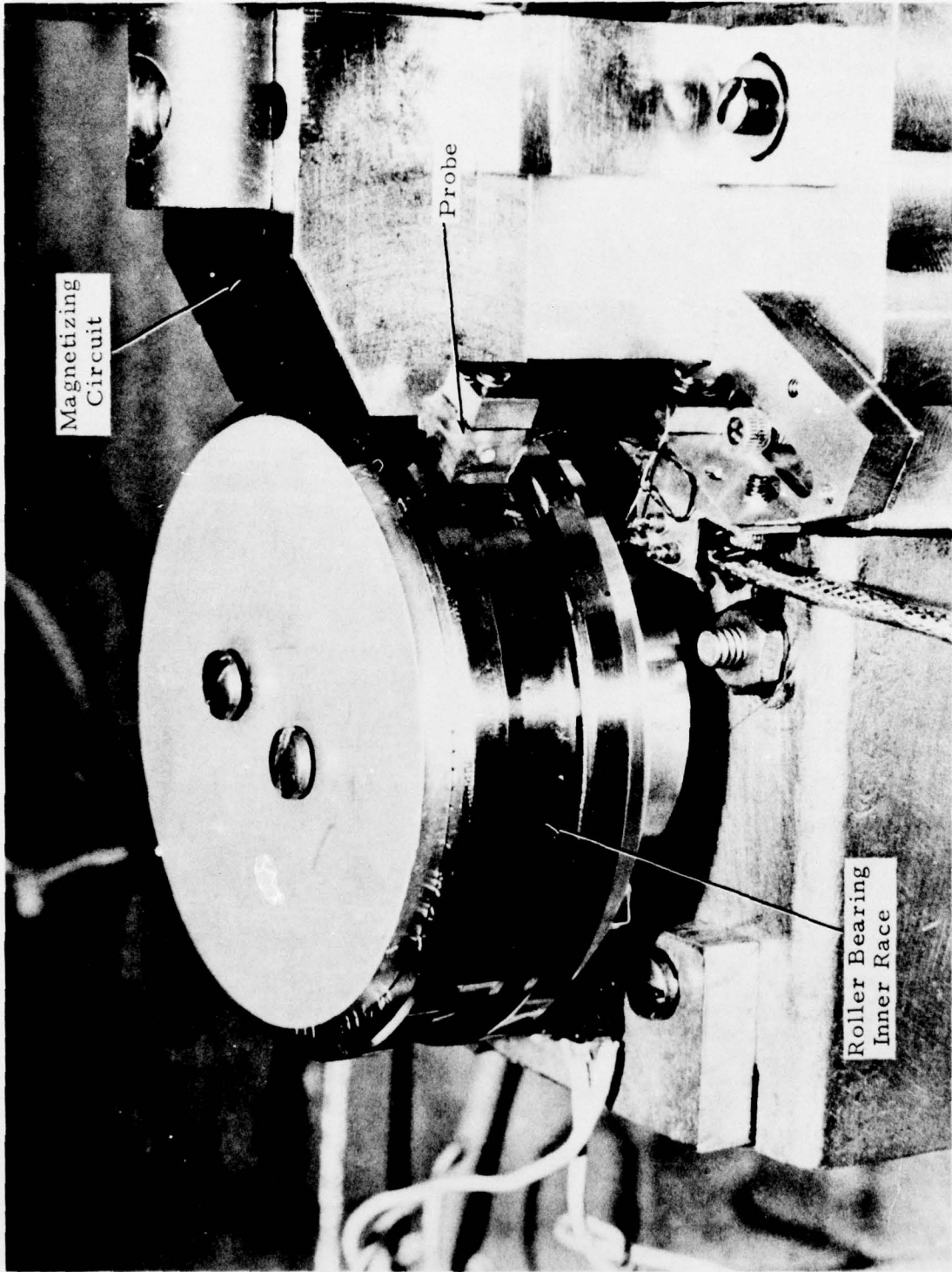


FIGURE A12. ROLLER BEARING RACE, PROBE, AND MAGNET POLE PIECE ARRANGEMENT USED FOR CONTINUOUS BARKHAUSEN EXPERIMENTS

4012

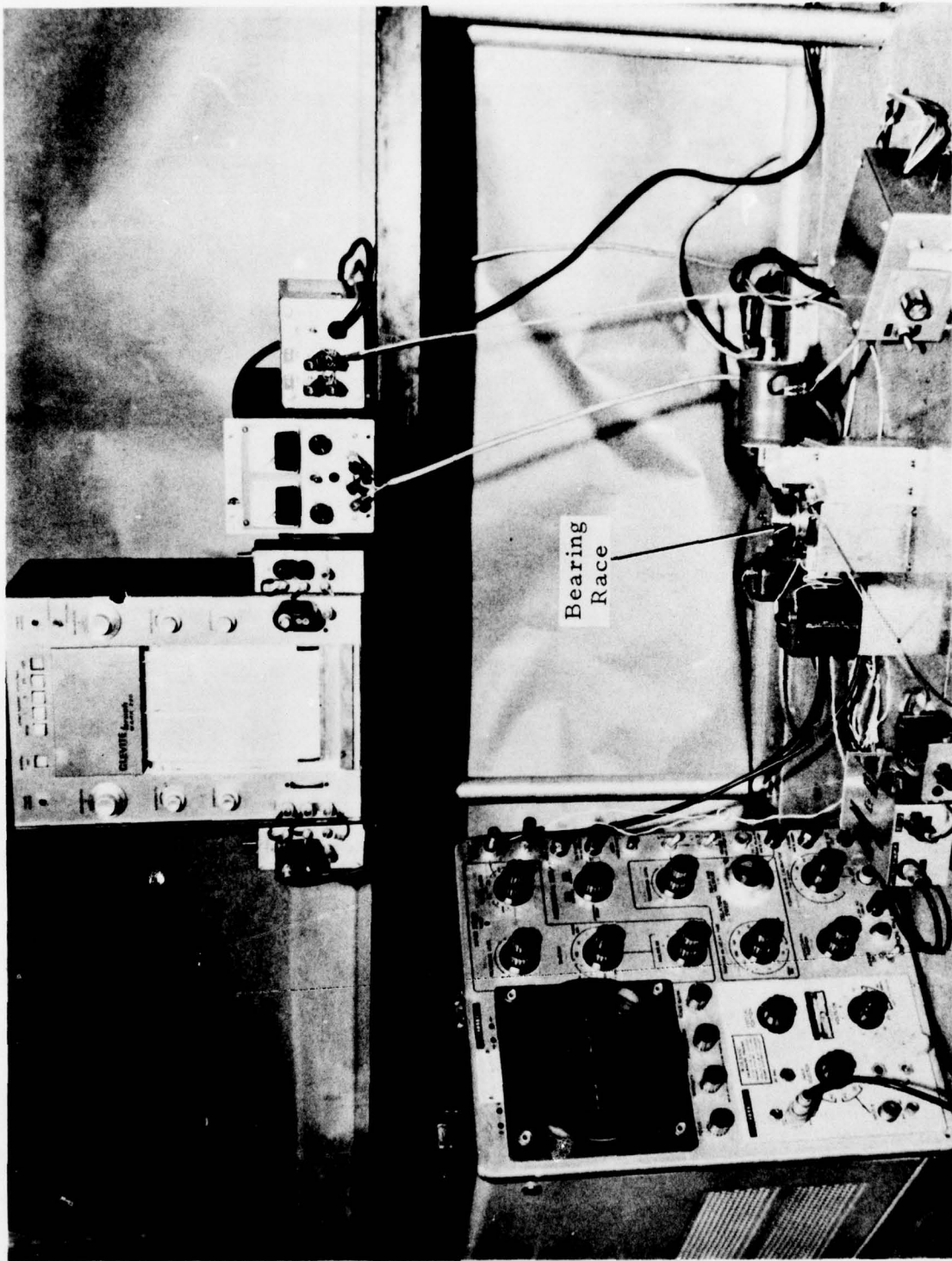


FIGURE A13. CONTINUOUS BARKHAUSEN APPARATUS FOR ROLLER BEARING RACE

level of continuous Barkhausen increases to a maximum and then decreases with further increases in magnetizing current; a similar behavior with magnetizing current was noted (but not illustrated) for the annealed 4130 steel flat specimen. In the case of the roller bearing race, when a magnetizing current exceeding that for maximum continuous Barkhausen amplitude was applied, a "pit-type" signal (pointed out by the arrow in Figure A11d) on top of the continuous Barkhausen was noted which was found to correlate with the manufactured indent. Investigations were carried out to verify that the indent signal was a Barkhausen noise signal and not a magnetic perturbation type indication. Record e in Figure A11 shows both the processed and unprocessed Barkhausen signal from the surrounding material, via Barkhausen signal, is significant since it offers the future possibility of a critical appraisal of indentation and brinelling in bearing races.

Although the continuous Barkhausen results were very encouraging and careful consideration was given to this approach, the conventional Barkhausen approach was selected to be implemented in the bearing inspection system. This decision was based on the fact that essentially all existing Barkhausen noise data on "before" and "after" service bearings were obtained using the conventional Barkhausen approach. Furthermore, the most outstanding change in the conventional Barkhausen signature noted as a result of service was that in the vicinity of the leading edge of the signature, i. e. , formation of the "spike" signal; under similar conditions, the extent and kind of change in the continuous Barkhausen to be anticipated is unknown at the present time. In addition, the detailed relationships between the continuous and the conventional Barkhausen approaches are also unknown; based on current evaluations, indications are that the continuous Barkhausen phenomena is a complex one and little is known about the controlling parameters at this time.

Implementation of a conventional Barkhausen noise approach consisted of developing i) interface circuitry and computer hardware to facilitate programming of the magnetic perturbation drive motor system to acquire specified static circumferential locations, ii) signal amplifiers and processing of electronic circuits, and iii) circuits to facilitate the use of the magnetic perturbation magnetizing current source (and magnetizing coils) to provide a time-varying current for the Barkhausen noise inspection. Figure A14 shows a photograph of the preliminary prototype system and associated laboratory equipment used during the Barkhausen circuit development phases of the work.

During setup and alignment of the fixturing for the prototype (CCAD) system, an unusual Barkhausen signature was noted on the accessory set of the 205-040-246 and 204-040-346 inner bearing race. Delivery

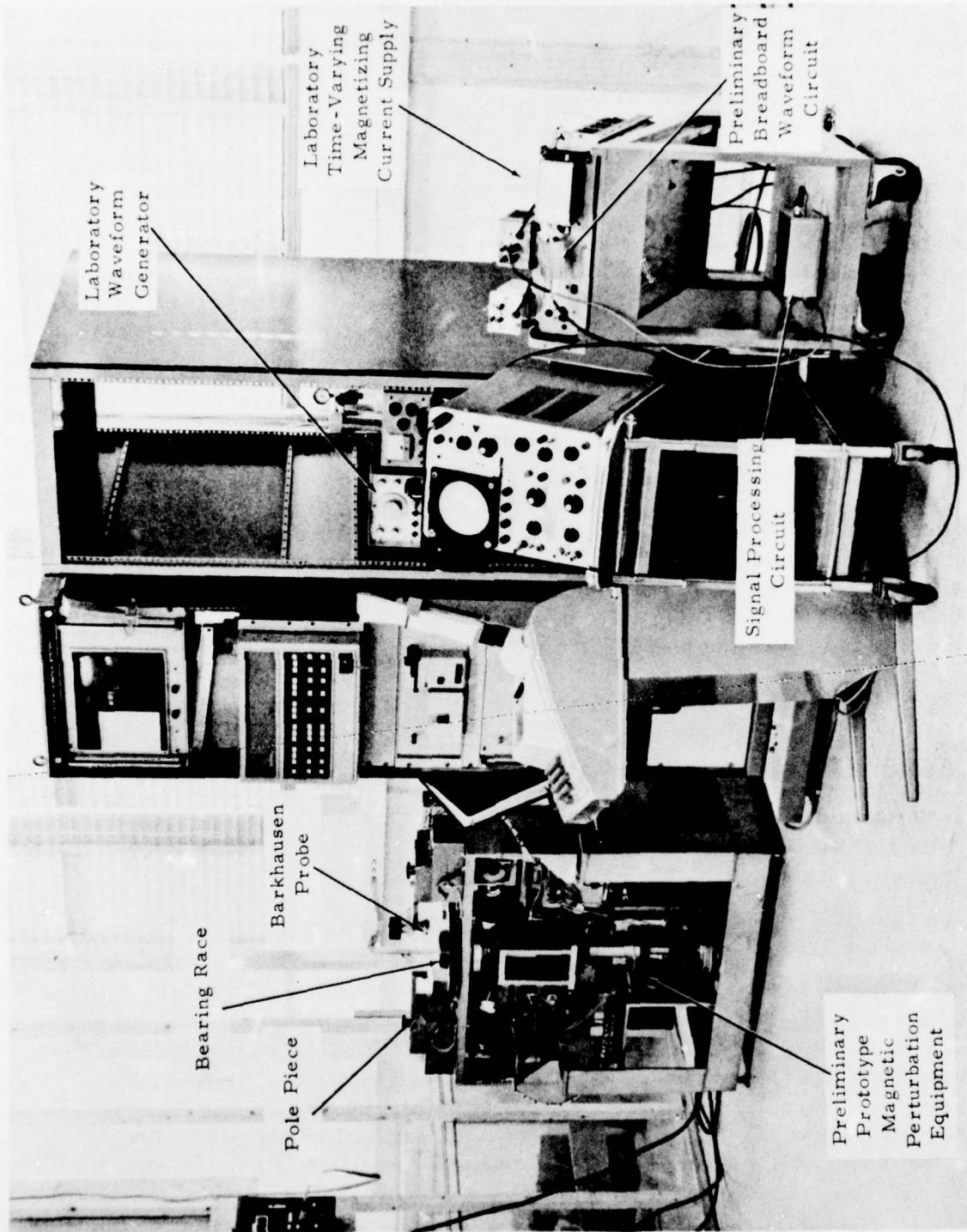
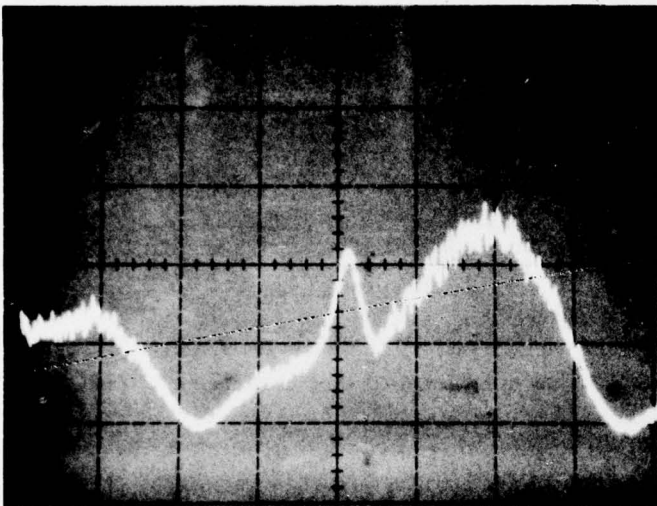


FIGURE A14. OVERALL VIEW OF PRELIMINARY PROTOTYPE UNIT DURING DEVELOPMENT OF BARKHAUSEN INSTRUMENTATION

of this accessory set was postponed pending further checks on this Barkhausen signature. Furthermore, during operational checkout of the preliminary prototype unit, an unusual Barkhausen signature was noted on the 1-300-015 outer race which contained shape characteristics very similar to those observed on the 204-040-346/205-040-246 inner race accessory set. This anomalous Barkhausen signature shape was not noted for the same 1-300-015 outer race on the prototype (CCAD) system. In-depth investigations were made by changing out Barkhausen probe, preamplifier, and other signal system components several times but the improper Barkhausen signature persisted. However, when the unprocessed Barkhausen signature was viewed on a much expanded time scale, a periodic signal of approximately 200 kHz was observed to occur in synchronization with the time-varying applied magnetic field. Subsequent investigation revealed that the probe coupling air was inducing a high frequency mechanical vibration (~ 200 kHz) in the Barkhausen probe pickup coil which resulted in the generation of an electrical signal in the Barkhausen probe via the time-varying applied magnetizing field. The influence of the probe coupling air is illustrated by the records in Figure A15. Note the anomalous Barkhausen signature in the upper record with normal air coupling and the absence of the anomalous signal component when the probe air is turned off (see lower record). It was concluded that i) in those cases where the anticipated Barkhausen signature shape is obtained, all probe coil turns were bonded to the probe coil form, and ii) in those cases where an improper shaped signature was obtained, the face turns of the probe coil were not tightly bonded to the coil form. Based on this rationale, new Barkhausen probes were fabricated where all coil turns were carefully bonded to the coil form. The results of this effort in alleviating the air-induced mechanical vibration problem was previously illustrated in Figure 12 in this report.

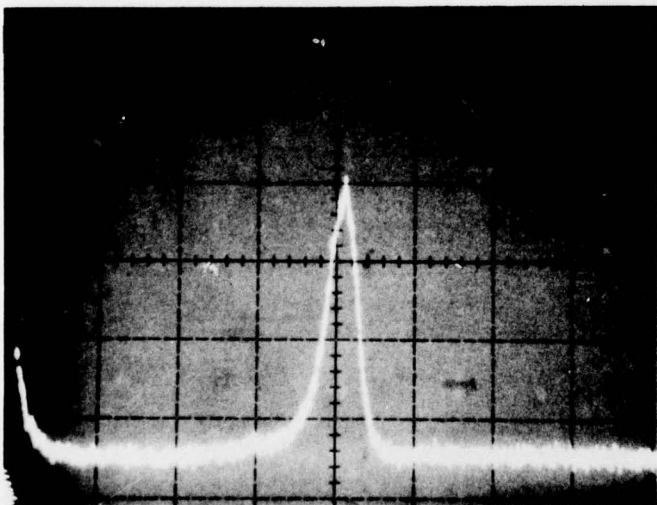
4009



Normal Air Coupling

Vertical Sensitivity 50 mV/div

Horizontal Sweep 0.2 sec/div



Probe Air Off

Vertical Sensitivity 50 mV/div

Horizontal Sweep 0.2 sec/div

FIGURE A15. BARKHAUSEN NOISE RECORDS ILLUSTRATING THE INFLUENCE OF AIR-INDUCED MECHANICAL VIBRATION ON BARKHAUSEN SIGNATURES

DISTRIBUTION LIST

No. of Copies	To
12	Commander, Defense Documentation Center, Cameron Station, Building 5, 5010 Duke Street, Alexandria, Virginia 22314
	Commander, U. S. Army Materiel Development and Readiness Command, 5001 Eisenhower Avenue, Alexandria, Virginia 22333
1	ATTN: DRCMA-E
1	DRCQA
1	DRCQA-E
	Commander, U. S. Army Aviation Systems Command, P. O. Box 209, St. Louis, Missouri 63166
1	ATTN: DRSAV-F
5	DRSAV-FE
1	DRSAV-LEP
1	DRSAV-LR
1	DRSAV-EF
1	DRCPM-IAP-T
1	DRCPM-CH47M
1	DRCPM-CO
1	DRCPM-AAH
1	DRCPM-UA
	Commander, Corpus Christi Army Depot, Corpus Christi, Texas 78419
15	ATTN: DRSAV-FESI (Mr. Bull)
1	DRXAD-G
1	DRXAD-Q
1	DRXAD-M
1	DRXAD-E
	Commander, Defense Industrial Supply Center, 700 Robbins Avenue, Philadelphia, Pennsylvania 19111
1	ATTN: DISC-MCB (Mr. Sweeney)
1	DISC-SCAC (Mr. Guerra)
1	DISC-S (Mr. Merlo)
	Commander, Defense Supply Agency, Cameron Station, Alexandria, Virginia 22314
1	ATTN: DCAS-QEM (Mr. Vibbert)
	Director, Eustis Directorate, U. S. Army Mobility R&D Laboratory, Fort Eustis, Virginia 23604
1	ATTN: SAVDL-EU-TAP (J. Lane)

No. of Copies	To
	Commander, U. S. Army Tank-Automotive Materiel Readiness Command, Warren, Michigan 48090
1	ATTN: DRSTA-RSEM (R. Biskner)
1	DRSTA-QE
1	DRCPM-CT
1	DRCPM-HT
1	DRCPM-M60TD
1	DRCMP-M60TP
1	DRCPM-M113
	Commander, U. S. Army Tank-Automotive Research and Development Command Warren, Michigan 48090
1	ATTN: DRDTA-J
1	DRDTA-JE
1	DRCPM-GCM
1	DRCPM-FV
1	DRCPM-MCV
	Commander, Naval Air Rework Facility, Naval Air Station, North Island, San Diego, California 92135
1	ATTN: Code 343 (D. Stanley)
	Commander, Naval Air Rework Facility, Naval Air Station, Norfolk, Virginia 23511
1	ATTN: R. Martucci
	Commander, Naval Air Systems Command, Washington, D. C. 20361
1	ATTN: Code AIR 52022 (R. Retta)
1	Code AIR 52032E (P. Weinberg)
1	Code AIR 53374 (J. McHale)
1	Code AIR 530323 (G. Norman)
	Commander, Naval Ship Engineering Center, Center Building, Prince George's Center, Hyattsville, Maryland 20782
1	ATTN: Code 6148D (J. Deller)
	Commander, Naval Ammunition Depot, Crane, Indiana 47522
2	ATTN: Code 7051 (K. Rush/R. Cron)
	Commander, Naval Air Development Center, Warminster, Pennsylvania 18974
1	ATTN: Code 30212 (N. Rebuck)
1	Code 30212 (A. Ankeny)
	Commander, Naval Ordnance Station, Indianhead, Maryland 20640
1	ATTN: Code 6111 (G. McKnight)
1	Code 6111 (S. Brennan)

No. of Copies	To
1	Commander, Naval Air Rework Facility, Marine Corps Air Station, Cherry Point, North Carolina 28533 ATTN: Code 332 (J. Cunningham)
1	Commander, Air Force Aeronautical Systems Division, Wright-Patterson Air Force Base, Ohio 45433
1	ATTN: ASD/ENFEM (P. Smith)
1	ASD/ENESS (E. McPherson)
1	ASD/ENFIP (J. Andres)
1	Commander, Air Force Air Propulsion Laboratory, Wright-Patterson Air Force Base, Ohio 45433 ATTN: AFAPL/SFL (R. Dayton)
1	Commander, Warner Robbins Air Logistic Center, Robbins Air Force Base, Georgia 31098
1	ATTN: MEMI (Capt. Dammann)
1	MMIRDA (W. Webb)
2	MMSSM (Glenco/Couch)
1	Commander, Oklahoma City Air Logistic Center, Tinker Air Force Base, Oklahoma 73145 ATTN: MMPR (N. Kirby)
1	Commander, Army Research Office Box CM, Duke Station, Durham, North Carolina 27706 ATTN: Mr. G. Mayer
1	Commander, U. S. Army Troop Support Command, 430C Goodfellow Boulevard, St. Louis, Missouri 63120
1	ATTN: DRSTS-Q
1	DRSTS-QR
1	DRSTS-M
1	Commander, U. S. Army Mobility Equipment Research and Development Center, Fort Belvoir, Virginia 22060
1	ATTN: DRXFB-T
1	DRXFB-TQ
1	DRXFM-M
1	Commander, U. S. Army Test and Evaluation Command Aberdeen Proving Ground, Maryland 21005
2	ATTN: DRSTE-RM
2	DRSTE-ME (Wise/Champion)

No. of Copies	To
1	Commander, Aberdeen Proving Ground, Aberdeen, Maryland 21005 ATTN: STEAP-MF-M STEAP-MF-G (Huddleston)
1	Commander, Anniston Army Depot, Anniston, Alabama 36202
1	ATTN: DRXAN-Q
1	DRXAN-M
1	Commander, Letterkenny Army Depot, Chambersburg, Pennsylvania 17201
1	ATTN: DRXLE-Q
1	DRXLE-M
1	Commander, New Cumberland Army Depot, New Cumberland, Pennsylvania 17070
1	ATTN: DRXNC-Q
1	DRXNC-M
2	Director, Army Materials and Mechanics Research Center, Watertown, Massachusetts 02172
1	ATTN: DRXMR-PL
1	DRXMR-CT
1	DRXMR-PR
1	DRXMR-M
1	DRXMR-EM (P. Fopiano)
1	DRXMR-L (R. Chait)
15	DRXMR-MI (H. Hatch)
1	DRXMR-AP

Inspected
by